

1 **Impact of Eurasian autumn snow on the winter North Atlantic**  
2 **Oscillation in seasonal forecasts of the 20<sup>th</sup> century.**

3

4 Martin Wegmann<sup>1,2,3</sup>, Yvan Orsolini<sup>4</sup>, Antje Weisheimer<sup>5,6</sup>, Bart van den Hurk<sup>6,7</sup> and Gerrit  
5 Lohmann<sup>3</sup>

6

7 <sup>1</sup>Institute of Geography, University of Bern, Bern, Switzerland.

8 <sup>2</sup>Oeschger Centre for Climate Change Research, University of Bern, Bern, Switzerland.

9 <sup>3</sup>Alfred-Wegener-Institute, Helmholtz Center for Polar and Marine Research, Bremerhaven, Germany

10 <sup>4</sup>NILU–Norwegian Institute for Air Research, Kjeller, Norway

11 <sup>5</sup>National Centre for Atmospheric Science, Atmospheric, Oceanic and Planetary Physics, University of  
12 Oxford, Oxford, United Kingdom

13 <sup>6</sup>European Centre for Medium-Range Weather Forecasts, Reading, United Kingdom

14 <sup>7</sup>Deltares, Delft, The Netherlands

15

16

17 Corresponding author: Martin Wegmann, Institute of Geography and Oeschger Centre for Climate  
18 Change Research, University of Bern, Hallerstrasse 12, 3012 Bern, Switzerland. Email:  
19 martin.wegmann@giub.unibe.ch

20

21 **Key points**

22 Snow–atmosphere coupling, seasonal prediction, North Atlantic Oscillation, polar vortex, stratospheric  
23 warming, hindcast

24

25 **Abstract**

26 As the leading climate mode of wintertime climate variability over Europe, the North Atlantic  
27 Oscillation (NAO) has been extensively studied over the last decades. Recently, studies highlighted the  
28 state of the Eurasian cryosphere as a possible predictor for the wintertime NAO. However, missing  
29 correlation between snow cover and wintertime NAO in climate model experiments and strong non-  
30 stationarity of this link in reanalysis data is questioning the causality of this relationship.

31 Here we use the large ensemble of Atmospheric Seasonal Forecasts of the 20th Century (ASF-20C)  
32 with the European Centre for Medium-Range Weather Forecasts model, focusing on the winter season.  
33 Besides the main 110-year ensemble of 51 members, we investigate a second, perturbed ensemble of  
34 21 members where initial (November) land conditions over the Northern Hemisphere are swapped from  
35 neighboring years. The Eurasian snow / NAO linkage is examined in terms of a longitudinal snow depth  
36 dipole across Eurasia. Subsampling the perturbed forecast ensemble and contrasting members with high  
37 and low initial snow dipole conditions, we found that their composite difference indicates more negative  
38 NAO states in the following winter (DJF) after positive west to east snow depth gradients at the  
39 beginning of November. Surface and atmospheric forecast anomalies through the troposphere and  
40 stratosphere associated with the anomalous positive snow dipole consist of colder early winter surface  
41 temperatures over Eastern Eurasia, an enhanced Ural ridge and increased vertical energy fluxes into the  
42 stratosphere, with a subsequent negative NAO-like signature in the troposphere. We thus confirm the  
43 existence of a causal connection between autumn snow patterns and subsequent winter circulation in  
44 the ASF-20C forecasting system.

45        **1. Introduction**

46        As the leading climate variability pattern affecting winter climate over Europe, the North Atlantic  
47        Oscillation (NAO) has been extensively studied over the last decades (Wanner et al., 2001; Hurrell and  
48        Deser, 2010; Moore and Renfrew, 2012; Deser et al., 2017). The NAO state strongly impacts the  
49        hydroclimate as well as the ecological and socioeconomic conditions over major population clusters of  
50        Europe and North America. In its positive state, the NAO projects onto strong pressure gradients over  
51        the North Atlantic, strong westerly winds and mild but wet conditions for Central Europe. A negative  
52        winter NAO is connected to a southwardly displaced Atlantic jet stream, weaker westerlies and cold,  
53        dry conditions for Central Europe. The NAO also shows a distinct quadrupole signature in surface  
54        temperature straddling the Atlantic, with two opposite poles over northern Europe and Greenland  
55        /Labrador and an opposite pair further south over southern Europe/North Africa and the US East Coast.  
56        Recent cases of extreme negative NAO states (Wang and Chen, 2010; Lü et al., 2020), including the  
57        winter 2020/2021, coincided with several extreme weather events across the Northern Hemisphere,  
58        including cold air outbreaks with record snowfall at locations over Southern and Northern Europe, as  
59        well as eastern parts of Canada and the United States (Blunden and Boyer, 2021).

60        Improving seasonal to decadal predictions of the winter NAO is a high priority research for many  
61        weather and climate related research centres (Kang et al., 2014; Scaife et al., 2014, 2016; Smith et al.,  
62        2016; Dunstone et al., 2016; Athanasiadis et al., 2017; Weisheimer et al., 2017; Baker et al., 2018;  
63        Weisheimer et al., 2019). Despite its stochastic behaviour, the NAO state was shown to be modulated  
64        by slowly varying components of the climate system, carrying the climate state “memory“ across  
65        months or even seasons (Dobrynin et al., 2018; Meehl et al., 2021). Initially discussed by Cohen and  
66        Entekhabi (1999), recent studies have highlighted the potential of Eurasian autumn snow cover  
67        anomalies as a useful predictor for the boreal wintertime (December– January–February, DJF) NAO in  
68        empirical prediction models (Cohen et al., 2007, 2014; Cohen and Jones 2011; Peings et al., 2013; Tian  
69        and Fan 2015; Wang et al., 2017; Han and Sun 2018; Wegmann et al., 2020).

70        The causal chain behind the snow impact is hypothesized as follows: due to the radiative and  
71        thermodynamical properties of snow (Cohen and Rind 1991; Vavrus 2007; Dutra et al., 2011;  
72        Thackeray et al., 2019), a thicker snowpack is associated with coherent surface cooling. Cohen et al.  
73        (2007; see also Cohen et al., 2014; Henderson et al., 2018 for reviews) proposed a multi-step mechanism  
74        whereby this surface cooling leads to raised isentropic surfaces, triggering increased Rossby wave  
75        activity propagating upward and being absorbed in the stratosphere, warming it and subsequently  
76        weakening the polar vortex. The negative stratospheric Northern Annular Mode signal eventually  
77        propagates down into the troposphere and to the surface where it projects onto a negative NAO.

78        Investigating the robustness of this mechanism is challenged by several elements. Observational studies  
79        analyzing statistical links are restricted by the relatively short length (a few decades) of comprehensive  
80        and complete snow cover observations. Using long-term reanalyses, recent studies showed substantial

81 non-stationary relationships between autumn Eurasian snow cover and the sign of the winter NAO over  
82 the span of the 20<sup>th</sup> century (Peings et al., 2013; Douville et al., 2016; Wegmann et al., 2020). Using  
83 shorter time scales, the probability of “cherry picking” a period of positive correlation and sampling co-  
84 variability with other climate system components increases considerably. Causes for the non-  
85 stationarity are still discussed, with possible influences from the Quasi-Biennial Oscillation (QBO), El  
86 Niño-Southern Oscillation (ENSO) or simply snow cover variance (Peings et al., 2017; O’Reilly et al.,  
87 2017; Tyrrell et al., 2018; Wegmann et al., 2020; Weisheimer et al., 2020). Disentangling co-variability  
88 is further challenged by the co-occurrence of increased Eurasian snow cover and increased Ural  
89 blocking frequency, questioning the lead-lag relationship between snow cover and blocking (Peings  
90 2019; Song and Wu, 2019; Santolaria-Otín et al., 2021). Moreover, a variety of temporal and spatial  
91 snow cover indices used among the different studies obstructs direct comparisons. Nevertheless, recent  
92 studies point out that a November longitudinal snow cover dipole across Eurasia shows the strongest  
93 statistical link to the DJF NAO state (Gastineau et al., 2017; Han and Sun 2018; Santolaria-Otín et al.,  
94 2021).

95 Analyzing the snow → NAO mechanism in modelling experiments is challenged by short-comings of  
96 the current Atmospheric or Atmosphere-Ocean General Circulation Models (AGCMs or AOGCMs)  
97 regarding snow-atmosphere feedbacks (Santolaria-Otín and Zolina 2020). Most of the free-running  
98 Coupled-Model Intercomparison Project (CMIP) models do not capture the statistical snow-NAO link  
99 found in reanalyses data (Hardimann et al., 2008; Furtado et al., 2015; Gastineau et al., 2017). On the  
100 other hand, when large snowpack anomalies are prescribed through nudging or imposed as initial  
101 conditions, several AGCM experiments showed promising results for identifying several to all steps of  
102 the proposed mechanism (Gong et al., 2003; Fletcher et al., 2009; Peings et al., 2012; Tyrrell et al.,  
103 2018).

104 Some of the current-generation subseasonal-to-seasonal or seasonal coupled prediction models also  
105 seem to catch parts of the mechanism chain, specifically negative temperature anomalies associated  
106 with a thicker snowpack (Orsolini et al., 2013; Diro and Lin, 2020) as well as an enhanced wave activity  
107 generating upward fluxes into the stratosphere associated with ridging over Eurasia (Orsolini et al.,  
108 2016; Li et al., 2019; Garfinkel et al., 2020), although several models failed to simulate that ridging in  
109 Garfinkel et al. (2020). The subsequent stratosphere-troposphere coupling influencing the surface  
110 Arctic Oscillation also tended to be weak to non-existent in most models. These studies have been  
111 limited to the recent decades and, consequently, confidence in the robustness of the mechanism across  
112 spans of decades is still low and needs to be strengthened (Garfinkel et al., 2020).

113 To disentangle the issues of non-stationarity (found in observations) and causality (found in models),  
114 we base our investigation on a 110-year long (1901-2010) ensemble seasonal prediction experiment,  
115 which consists of the historical seasonal hindcasts using ECMWF’s atmosphere-only model, called  
116 “ASF-20C” (Weisheimer et al., 2017). This 51-member ensemble of hindcasts with four start dates per



117 year and a length of 4 months has been used in several studies on the predictability of the NAO and  
118 other climate patterns (e.g., O'Reilly et al., 2017; Parker et al., 2019; Weisheimer et al., 2019;  
119 Weisheimer et al., 2020; O'Reilly et al., 2020). To investigate the influence of land surface conditions,  
120 in this case snow cover, on the evolution of the atmospheric state throughout the season, we use a novel,  
121 21-member twin set of the ASF-20C forecasts with perturbed initial land conditions. This dataset was  
122 used as a pilot experiment in the context of the Land Surface, Snow and Soil moisture Model  
123 Intercomparison Program LS3MIP (Van den Hurk et al., 2016), aimed at reproducing land surface  
124 potential predictability experiments as described by Dirmeyer et al. (2013). We aim to address the  
125 question of causality, pathway, stationarity and seasonal evolution of the proposed mechanism of the  
126 snow-stratosphere-troposphere linkage over decadal to centennial time scales.

127 This paper is organized as follows. Sect. 2 describes the data and methods used. In Sect. 3, we show  
128 winter evolution of climate anomalies for the different initialization runs and contrast them with  
129 observed anomalies. The results are discussed in Sect. 4 and finally summarized in Sect. 5.

130

## 131 2. Data and Methods

### 132 a. Climate reanalysis and reconstruction

133 We use the European Centre for Medium-Range Weather Forecasts (ECMWF) product ERA-20C  
134 (ERA20C; Poli et al., 2016) to investigate pre-conditions and the initialization of the seasonal  
135 predictions, to compute the DJF NAO index as well as to create a Eurasian snow dipole index. ERA-  
136 20C only assimilates surface pressure and marine wind observations, with sea surface temperature  
137 (SSTs) boundary conditions taken from the HadISST2.1.0.0 datasets (Rayner et al., 2003). ERA-20C  
138 was found to represent interannual snow variations over Eurasia remarkably well. For an in-depth  
139 discussion of its performance and the technical details concerning snow computation, see Wegmann et  
140 al., (2017b). Due to the a-forementioned statistical impact for the winter NAO evolution, we focus on  
141 the November Eurasian snow dipole index as a predictor for the following NAO state (Gastineau et al.,  
142 2017; Han and Sun 2018; Santolaria-Otín et al., 2021). Following Han and Sun (2018) who explicitly  
143 selected western and eastern domains because of the high co-variance with DJF NAO, we calculate the  
144 index over the period 1901–2010 by averaging snow depths over the western domain (30°-60°E, 48°N-  
145 58°N) and the eastern domain (80°-130°E, 40°-56°N), eventually subtracting the western domain from  
146 the eastern domain to derive the west-east snow depth gradient. Hence, a positive snow index indicates  
147 higher snow depths in the eastern domain and a positive longitudinal snow depth gradient. The index is  
148 normalized and linearly detrended with respect to the overall period. To comply with the initialization  
149 date of 1<sup>st</sup> of November for the seasonal hindcasts, we calculate the index for 1<sup>st</sup> of November instead  
150 of November mean snow (Figure 1a). Even though Han and Sun (2018) calculated the dipole index  
151 using snow cover, we used snow depth since ERA-20C provides snow depth as the actual prognostic  
152 variable. We hence refrained from using empirical rules to convert snow depth to snow cover. We found  
153 the index based on snow depth to be virtually identical (also see Supplementary Figure S1) to the index  
154 using snow cover (see also Wegmann et al., 2020 for more insights).

155 To compute the winter NAO index, we normalize the first Empirical Orthogonal Function of ERA-20C  
156 DJF sea level pressure (SLP) for the region (90°-50°E, 20°-80°N). We use the same approach to  
157 calculate the NAO DJF index based on the seasonal hindcasts and compare those with the reconstructed,  
158 independent DJF NAO index by Jones et al., (1997) from the Climate Research Unit (CRU).

### 159 b. Seasonal prediction experiments

160 Additionally, we use atmospheric seasonal retrospective hindcasts covering the 110-year period 1901-  
161 2010 of ERA-20C with 51 ensemble members of the ASF-20C hindcasts (hereafter ASF-20C CTL)  
162 (Weisheimer et al., 2017). The atmospheric model used for the 4-month hindcasts is the ECMWF  
163 Integrated Forecast System Version CY41R1 and is initialized at four start dates per year (1<sup>st</sup> of Feb,  
164 May, Aug and Nov) with ERA20C land and atmospheric conditions. It uses the same lower boundary  
165 conditions for SST and sea ice as ERA-20C. Here, we only use hindcasts initialized on the 1<sup>st</sup> of  
166 November. The horizontal spectral resolution of the model of T255 is similar to ECMWF's previous

167 operational system System 4 (Molteni et al., 2011) and corresponds to a grid length of approximately  
168 80 km. The model has 91 vertical levels and a top at 0.01 hPa. The ensemble has been created by  
169 perturbing each member through the stochastic physics schemes to represent model uncertainties in a  
170 similar way as the a-forementioned System 4.

171 To investigate the impact of Eurasian snow depth we use an additional set of perturbed hindcasts, based  
172 on a 21-member subset of the ASF-20C CTL experiment (hereafter, the “Experiment” or ASF-20C  
173 EXP). Each member run is initialized with different land surface conditions, sampled from the  
174 neighbouring 20 years. For example, the range of land surface conditions for the 21-member ensemble  
175 forecast initialised on 1<sup>st</sup> of November 1950 spans the land surface conditions of the years 1940–1960:  
176 member 01 is initialized with the land surface conditions of 1940, member 02 of 1941, member 03 of  
177 1942 and so forth. For the beginning and ending ten years of the hindcast dataset, the land surface  
178 conditions are sampled from the closest 21 neighbouring years within the dataset. Here, land surface  
179 conditions include the entire land state, including soil moisture, snow depth and soil temperatures. We  
180 argue that for investigating northern hemisphere climate anomalies of the 1<sup>st</sup> of November initialization,  
181 snow depth has by far the largest impact on atmospheric dynamics compared to soil moisture and soil  
182 temperatures, thus allowing us to attribute the differences to snow changes. The main bulk of the  
183 experiment data has a monthly resolution, and daily data is only available for selected variables and  
184 three tropospheric levels. After initialization, oceanic components like SSTs and sea ice are  
185 prescribed and based on observations among all members in ASF-20C CTL and ASF-20C EXP.

186 Taking advantage of the shuffled initial land conditions of ensemble members in ASF-20C EXP, we  
187 subsample members with positive or negative initial Eurasian snow dipole (Figure 2). This conditional  
188 sampling approach has been used when testing the sensitivity of extended range forecasts to soil  
189 moisture (Koster et al., 2011; van den Hurk et al., 2012) or to snow initial conditions (Li et al., 2019;  
190 Garfinkel et al., 2020). For each start date, we can identify those members with positive or negative  
191 initial snow dipole indices, corresponding to different years of the shuffled land initialisation. We  
192 further proceed with compositing these two selected sets. Due to the decadal variability in the November  
193 snow cover, the amount of “high snow dipole members” (positive dipole index) and “low snow dipole  
194 members” (negative dipole index) varies throughout the 110 years. There might be periods when a  
195 majority of the neighbouring 20 years shows a positive snow dipole index and other periods when a  
196 minority does. To avoid this variation of the composited ensemble size across the years, we only use  
197 the five ensemble members with the most positive and most negative initial Eurasian snow dipole,  
198 creating two ensemble means (each of size N=5), namely a high snow dipole ensemble-mean and low  
199 snow dipole ensemble mean, for each winter through the 110-year period.

200 It should be noted that the absolute magnitude of the ensemble-mean snow differences is still changing  
201 from year to year. For example, the most positive snow dipole for the period 1910–1930 might be lower

202 than in the time window 1980–2000, and the same applies for negative dipole indices. Due to the  
203 definition of the ASF-20C EXP, this setup is unavoidable, but it also allows for realistic magnitudes of  
204 snow forcings and for incorporating a realistic natural variability into the experiment. The (5-member)  
205 ensemble-mean difference (Figure 3a) displays a snow depth increase of 1-2 cm over Central and  
206 Eastern Siberia, together with a 0.2-1 cm snow depth decrease over Western Russia, as expected from  
207 the snow dipole definition. Concomitant negative anomalies (1-2 cm snow depth) nevertheless extend  
208 outside of the dipole definition domains to more northern latitudes, e.g., over Western Russia and the  
209 Russian Far East, or over the coastal mountain ranges of the North American Pacific Northwest. Note  
210 that the two domains forming the dipole are in snow transition zones, where the snow cover is rare on  
211 November 1<sup>st</sup> and shows some variability (Figure 3b-c). The dipole positive phase corresponds to  
212 anomalously high snow depths over Eastern Eurasia, where the ERA20C snow depth climatology  
213 indicates a few centimeters of snow. It also corresponds to anomalously low snow over the west of  
214 Russia, in regions with no to rare snow cover in the ERA20C November 1<sup>st</sup> climatology. The eastern  
215 domain partly covers the Mongolian Plateau region which was shown to exert a strong impact of the  
216 wintertime wave fluxes in the stratosphere (White et al., 2017).

217 If not stated otherwise we compute differences between the 5-member ensemble means of the “high  
218 snow dipole” and “low snow dipole” in ASF-20C-EXP as well as differences of each ensemble mean  
219 relative to the ensemble mean of ASF-20C CTL. We compute significance using a two-sided Student’s  
220 t-test.

### 221 3. Results

#### 222 a. DJF NAO comparison

223 Figure 1b shows the time series of the normalized reconstructed (i.e., based on station data), reanalysed  
224 and predicted winter NAO state for the period 1901–2010. Unsurprisingly, the ensemble means of the  
225 ASF-20C CTL and ASF-20C EXP hindcasts show reduced temporal variance compared to the  
226 observation-based NAO datasets. However, single realizations and member spread of the CTL and EXP  
227 runs cover the whole range of variability displayed by the observation-based product (see also  
228 Supplementary Figure S2).

229  
230 The correlation between the ERA-20C and CRU NAO index is 0.83, indicating that the EOF approach  
231 is a good approximation of the station-based index. It should be noted that the DJF average has a higher  
232 correlation between hindcasts and reanalyses than the individual months within the season (see  
233 Supplementary Table S1).

234 The ASF-20C CTL ensemble mean DJF hindcasts achieves an overall correlation of 0.33 with the CRU  
235 NAO reconstruction for the complete time period, with ASF-20C EXP having a nearly identical  
236 correlation (0.34). This near-identical correlation is expected given that the land state perturbations

237 across the 21 members are two-sided. Differences between the predicted NAO index of ASF-20C CTL  
238 and EXP ensemble means are generally small, with the NAO indices having the same sign during most  
239 winters. The correlation between CTL and EXP is 0.8 for the 110-year period. The slightly stronger  
240 variability of ASF-20C EXP can partly be attributed to the reduced ensemble size.

241 Contrasting the (initial) high-dipole and low-dipole composites constructed from the ASF-20C EXP  
242 ensemble, we see decadal variability in the difference of winter-mean NAO (Figure 1c&d). The first  
243 two decades of the 20<sup>th</sup>-century are characterized by rather strong negative NAO responses to a strong  
244 positive snow dipole. This is followed by two decades spanning the early twentieth century Arctic  
245 warming (Polyakov et al., 2003), which shows the opposite response: A strongly positive west-east  
246 snow depth gradient, as depicted in Figure 3, leads to more positive NAO-like states compared to a  
247 weak west-east snow depth gradient. After several decades with changing responses to the snow  
248 anomaly between the two ensembles, eventually the 21<sup>st</sup>-century starts with a weak negative NAO  
249 response to a strong positive snow dipole. Averaged over the whole period, the high snow dipole  
250 ensemble shows a slightly stronger negative NAO response: 51 cases of positive NAO response versus  
251 59 cases of negative NAO response. For more extreme NAO states (1 SD exceedance), the difference  
252 is more pronounced: 18 versus 29, and for 2 SD exceedance, 2 versus 9. Possible reasons for the decadal  
253 response to the snow forcing will be considered in the discussion section.

#### 254 **b. Regression analysis**

255 Previous studies showed that regressing observed boreal winter zonal-mean temperature and zonal wind  
256 anomalies onto an observed Eurasian autumn snow index reveals a significant stratospheric warming  
257 and slow-down of the polar vortex starting in November, migrating down towards the tropopause until  
258 February (Wegmann et al., 2020). A similar relation between Eurasian snow and the polar stratosphere  
259 can be found in the dataset used here.

260 Figure 4 shows a strongly reduced polar vortex for the ERA20C autumn to winter climate anomalies  
261 regressed on the November snow dipole index. The zonal wind anomalies in the troposphere highlight  
262 a weakened polar jet and an increased subtropical jet, especially in January and February. The  
263 concurrent polar stratospheric warming signal moves towards the upper troposphere throughout the  
264 winter months, with peak warming at around 100 hPa in February.

265 Spatially, pressure anomalies regressed onto the November snow dipole index reveal that the  
266 geographical center of the stratospheric warming is located over the Canadian Arctic (Figure 5).  
267 Tropospheric pressure differences highlight a strong ridging over Western Russia and the Ural  
268 Mountains in December, which subsequently over the course of winter is shifted more towards  
269 Greenland and the Northern North Atlantic region, reflecting a negative NAO-like atmospheric state.  
270 This state is further supported by negative DJF SLP anomalies over Southern Europe and the  
271 Mediterranean region. Downstream of the Eurasian snow signal, a negative SLP anomaly is found over  
272

273 the Northern North Pacific. The question remains, if these patterns derived by the regression analysis  
274 are a result of co-variability, common climate drivers or causal physical processes.

### 275 **c. Spatial anomalies in the experiment**

276 In the following, we investigate the spatial differences in the atmospheric response associated with the  
277 high and low snow dipole ensemble means of ASF-20C EXP, focusing on the initial response in  
278 December as well as the average DJF response, as the November response is not yet significant for  
279 almost all climate variables.

280 Figure 6a&b shows stratospheric geopotential heights anomalies at 10 hPa. In December, a significant  
281 negative anomaly formed above Eurasia, corresponding to a polar vortex displacement toward the  
282 Eurasian sector and a high over Alaska (albeit not significant), as commonly found during stratospheric  
283 warming events. Over the course of the winter, this pattern develops into increased geopotential heights  
284 over the Arctic with significantly reduced geopotential heights over the extratropics, albeit only  
285 significant over Southern Europe and the Caucasus.

286 To better understand the wave activity flux into the stratosphere, we investigated the meridional eddy  
287 heat flux at 100 hPa, which is proportional to the vertical component of the wave activity flux (Figure  
288 6c): it highlights a wave train of circumpolar anomalies in December (hence, following the surface  
289 signal forcing in November) with significant positive anomalies over the Ural mountains, eastern North  
290 Pacific and the European part of the North Atlantic and negative anomalies over Central and Northern  
291 Europe and along the North American Pacific coast. The average DJF response highlights a circumpolar  
292 wave-train but shows significant anomalies only for the increased northward heat flux over the northern  
293 North Atlantic.

294 Tropospheric circulation anomalies are depicted for geopotential heights at 500hPa in Figure 6e&f. In  
295 December, a strong positive anomaly is located over the Barents-Kara Sea sector, with significantly  
296 negative anomalies up- and downstream. A second region of positive anomalies emerges at the  
297 Canadian Atlantic coast. Both regions match the significant positive anomalies in the 100 hPa heat flux  
298 well. The averaged DJF anomalies highlight a negative mid-tropospheric NAO signal with significantly  
299 increased geopotential heights above Greenland and Iceland.

300 Sea level pressure anomalies largely mirror the 500 hPa geopotential height anomalies. The averaged  
301 DJF pattern only shows significant positive anomalies over the northern North Atlantic, but still projects  
302 onto a meridional pressure gradient characteristic of a negative NAO anomaly (Fig. 6h). It is important  
303 to note, that the absolute difference is rather small compared to interannual SLP variability. Anomalies  
304 between the two ensemble-means are less than 1 hPa. Even though this number can be assumed to be

305 smaller than in observational datasets due to the ensemble averaging process, it only constitutes about  
306 15% of the average 1901–2010 DJF SLP standard deviation over the Euro-Atlantic sector.

307 Due to its large variability, composites of the near-surface temperature are largely non-significant  
308 (Figure 6i&j). Yet, in December a clear cooling signal emerges over Central and Eastern Eurasia, as  
309 expected from the location of the positive snow anomalies at the time of forecast initialization. At the  
310 same time, eastern North America and south-eastern Europe show significant positive temperature  
311 anomalies, a result of northward heat advection at the eastern flanks of low-pressure anomalies (Figure  
312 6g). Averaged DJF 2m temperatures are significant only for Greenland and Eastern Eurasia, with the  
313 cooling over the latter a direct result of the persistence of the anomalously high initial snowpack.

314  
315

#### **d. Vertical anomalies in the experiment**

316 To get a better understanding on how the different land initial conditions impact the vertical distribution  
317 of temperature and zonal wind, Figure 7 shows meridional cross-section of the zonal-mean anomalies  
318 of zonal wind and temperatures from November to February.

319 While November anomalies (Figure 7) are overall insignificant, a strong snow dipole is associated with  
320 an increased polar vortex and cooler stratosphere. In December, zonal wind anomalies are indicative of  
321 the tropospheric subtropical jet shifted northward concurrent with a weak Arctic surface warming.  
322 Changes are substantial in January, when the stratospheric polar vortex is significantly weakened, with  
323 a slight increase in westerlies in the mid-troposphere. The corresponding temperature anomalies show  
324 a widespread stratospheric warming and negative anomalies in the lower Arctic troposphere. Eventually  
325 in February, the slow-down of westerlies is predicted to reach all the way down from the stratosphere  
326 into the troposphere. On the southern flank of these negative zonal wind anomalies, westerly winds are  
327 increasing, especially so in the stratosphere. The stratospheric warming signal migrates downwards to  
328 the lower stratosphere and tropopause layer. As the warming has migrated down, a stratospheric cooling  
329 is occurring aloft.

330 As a further confirmation, polar cap heights (Supplementary Figure S3) reveal a development of  
331 positive anomalies from the surface in December up to the stratosphere in January, migrating back to  
332 the troposphere in February. Note that the development of these anomalies is delayed compared to the  
333 one shown in the ERA20-C reanalyses (compare Figures 4 and 7) since initial atmospheric conditions  
334 are identical in the perturbed ensemble members.

335  
336

#### **e. Daily evolution of anomalies in the experiment**

337 To investigate the temporal evolution of important tropospheric anomalies, Figure 8 shows daily mean  
338 500 hPa GPH anomalies (high minus low snow dipole ensembles) averaged over 60-70°N. The  
339 Hovmöller diagram illustrates the Ural ridge developing only at the end of November going into

340 December and is preceding the development of the North Atlantic ridge, which is the main component  
341 of the negative NAO-like feature in our results. It should also be noted that the absence of meaningful  
342 anomalies during the first ten days of the composite difference again reflects the identical tropospheric  
343 anomalies arising from the pre-conditions. The anomalies generated by the end of November do indeed  
344 arise from the impact of snow cover differences and snow-atmosphere feedbacks.

345

#### 346 **f. Non-linearities in the snow forcing impact**

347 Two distinct non-linearities need to be considered. First, a non-linearity in the physical snow feedback:  
348 adding a few centimetres of snow in a snow-covered region will not change the radiative and  
349 thermodynamic properties of the already snow-covered land surface substantially (due to a saturation  
350 effect) but, by contrast, removing a few centimetres of snow might remove the snow layer altogether,  
351 changing drastically the albedo and thermodynamics of the surface-atmosphere boundary. This non-  
352 linearity may be important for the Rossby wave generation as air flows over the uplifted isentropes  
353 above the snow-covered area. The non-linear effect of snow cover saturation and the impact of the  
354 relative magnitude of regional surface cooling in our experiments is addressed by Figure 9. In years  
355 when the high minus low snow depth dipole EXP ensemble anomalies preceded a negative NAO  
356 anomaly (see Figure 1d for indication of years), the December cooling anomaly over Eastern Eurasia is  
357 much stronger than for the opposite case when it preceded a positive NAO anomaly. Concurrently, the  
358 formation of a Ural ridge anomaly is much more pronounced, flanked by troughs up and downstream,  
359 with positive eddy heat fluxes into the stratosphere over the Barents-Kara Sea and polar stratospheric  
360 warming. This supports the notion that adding an absolute amount of snow (in either of the two  
361 longitudinal domains) is not sufficient for the causal chain to be triggered. Instead, it is a large (in  
362 magnitude and extent) relative surface temperature impact of the additional snow that triggers the initial  
363 anomalous Rossby wave generation part of the hypothesized causal chain.

364 A second non-linearity is the asymmetrical role of the eastern and western domains of the snow dipole.  
365 Our subsampling of the ASF-20C EXP simulation allows to estimate the respective roles of these two  
366 domains. Interestingly, the difference between the low snow dipole ensemble mean and the CTL  
367 ensemble mean for DJF sea level pressure (Figure 10) reveals a much stronger response to a negative  
368 snow dipole (i.e., with high snow depths over Western Russia and low snow depths over Eastern  
369 Eurasia) than to the positive snow dipole (i.e., with high snow depths over Eastern Eurasia and low  
370 snow depths over Western Russia). The reason behind this is a combination of study design, the non-  
371 linearity of snow cover and the snow climatology of Eurasia. In Figure 10a, we compare the effect of a  
372 very non-climatological snow depth gradient to the impact of a climatological snow depth gradient and  
373 as such get a very strong response in SLP anomalies. This comparison equalizes or reduces the snow  
374 depth gradient and as a result very zonal flow occurs over high-latitudes. In Figure 10b, we compare  
375 the effect of a slightly increased (to the climatology) snow depth gradient to the impact of a



376 climatological snow depth gradient and as such, in addition to the weak impact of snow cover increase,  
377 get a weak to non-existent surface signal out of this experimental design.

378 By splitting up the 110 years of ASF-20C CTL (climatology) in two batches with high or low snow  
379 depth gradient initial conditions (1<sup>st</sup> November dipole index higher or lower than 0 based on Figure 1a)  
380 we can shed more light on those non-linearities and boost the signal of the high snow depth dipole EXP  
381 ensemble (Figures 10c-f). If we compare the high snow dipole EXP ensemble to CTL winter after a  
382 weak west-east snow depth gradients (dipole index below 0), the anomalies show slightly elevated SLP  
383 over the northern North Atlantic (Fig. 10f), albeit in much lower magnitude than for the opposite  
384 comparison (Fig. 10e) (see Supplementary Figure S4 for snow depth anomalies). A weak snow depth  
385 gradient seems to nearly always favour zonal flow (Figs. 10d,e,f) whereas increasing the gradient needs  
386 to overcome a higher threshold due to the climatology representing a natural west-east gradient already,  
387 even before the experiment treatment shows its impact. Nevertheless, anomalies between the high snow  
388 depth dipole and low snow depth dipole EXP ensembles show the effect of an increased west-east snow  
389 depth gradient, which does in fact support the formation of more negative NAO-like states.

390 In other words, the relative snow depth changes in our model world are much larger in the western  
391 domain, and as such, the western domain carries most of the signal in our analysis. A simple regression  
392 analysis with the CRU DJF NAO index and ERA20C November snow depth shows a similar result  
393 (Supplementary Figure S5). We find that a linear regression model using only the eastern domain snow  
394 depth variability for explaining DJF NAO shows less significance than a model only using the western  
395 domain snow depth variability. Using the west-east gradient shows the highest significance for  
396 predicting wintertime NAO, no matter if we use ERA20C derived NAO or station-based NAO.

397 That said, with the negative dipole corresponding to lower snow depths over the eastern domain  
398 (Mongolian Plateau and surroundings areas), our results are consistent with lessened wave fluxes into  
399 the stratosphere over this region which is the important orographic driver of climatological upward  
400 wave fluxes in winter (White et al., 2017).

#### 401 4. Discussion

402 We used a set of centennial ensemble seasonal hindcasts (ASF-20C) and a complementary set with  
403 perturbed land initial conditions (ASF-20C-EXP) to address some of the open questions regarding the  
404 relationship between Eurasian autumn snow cover and the state of the NAO in the following winter.  
405 Subsampling of the latter hindcasts set according to the initial value (on 1<sup>st</sup> of November) of a west-east  
406 snow dipole over Eurasia (Gastineau et al., 2017; Han and Sun, 2018) allowed us to determine the  
407 response over 110 winters.

408 The regression of stratospheric wind and temperature upon the snow dipole in ERA20C over the 1901-  
409 2010 period reveals a weakened stratospheric vortex in January and February, following a positive  
410 initial snow dipole. Even though the linear regression analysis represents a deterministic “single

411 member” approach resulting in different magnitudes and shorter response times, the seasonal evolution  
412 of the ASF-20C EXP high-low snow dipole anomalies similarly indicates a weakened polar vortex. It  
413 also supports the notion of a surface cooling over the Eastern domain anchoring a Ural ridge anomaly  
414 on its western flank in December (Figure 6e). This Ural ridge triggers an increased northward heat flux  
415 in the lower stratosphere, thereby reducing the polar vortex strength and increasing polar stratospheric  
416 temperatures. In January and February, the signal moves downwards into the troposphere where it  
417 evolves into a negative NAO anomaly. In general, these results agree with the framework proposed by  
418 Cohen et al., (2007) and the experiments with the ECMWF seasonal prediction model by Orsolini et al.  
419 (2016). The physical causal chain in our experiment is also in line with recent model studies  
420 investigating the impact of Eurasian snow on stratospheric warmings and possible surface climate  
421 anomalies (Lü et al., 2020; Cohen et al., 2021). However, it should be highlighted that the absolute  
422 ensemble-mean, time-average SLP signal, diagnosed as the conditional composite difference in ASF-  
423 20C EXP, is very small, less than 1 hPa. As mentioned before, this represents only a small fraction of  
424 the interannual SLP variability in the Euro-Atlantic region. Nevertheless, for single realisations of  
425 winter forecasts, this impact can be much higher. By design, we excluded the impact of sea ice on the  
426 NAO evolution, since SSTs and sea ice stay the same through time in all EXP members. We checked  
427 for significant tropical precipitation patterns in the high minus low anomalies for November and  
428 December as potential co-variates in driving an DJF NAO signal but found no coherent significance  
429 across tropical latitudes. As such, we exclude tropical rainfall as first order driver behind the EXP NAO  
430 response.

431 The role of the Ural ridge in the snow cover → NAO causal chain has been discussed and analysed in  
432 several recent studies (Peings 2019; Santolaria-Otín et al., 2020). Here we find that the Ural ridge is a  
433 pre-condition of predicted negative NAO winters in ASF-20 CTL (Supplementary Figure S6), together  
434 with a cold 2m temperature anomaly in Eastern Russia and a cold stratospheric polar vortex displaced  
435 over Eurasia, downstream of the Ural ridge. However, these initial conditions are subtracted out in the  
436 ASF-20C EXP high--low snow dipole composite difference, and we find that the composite difference  
437 indicates a reinforced Ural ridge (Figure 6e). We find the mid-troposphere Ural ridge is reinforced only  
438 at the end of November going into December, which precedes the formation of a North Atlantic ridge  
439 that prevails until February (Figure 8). This result indicates that the snowpack does indeed play a  
440 feedback role (see also Orsolini et al., 2016). Thus, we propose that the relation between the Ural ridge  
441 and Eurasian snow cover consists of a mutual interaction: the circulation anomaly associated to a pre-  
442 existing Ural ridge shovels cold polar air southwards along its eastern flank, allowing for a deeper  
443 snowpack to form over Eastern Eurasia. In addition to this process (Figure 9c), our analysis reveals that  
444 the snow cover anomaly reinforces the Ural ridge, allowing for increased wave flux into the  
445 stratosphere. This location of a tropospheric ridge interferes constructively with climatological

446 stationary wave-1 and wave-2 patterns (Garfinkel et al., 2010) and seems to be key for a skilled forecast  
447 of the polar winter stratosphere (Portal et al., 2021).

448 Furthermore, the high minus low composite highlights a subpolar North Pacific surface and mid-  
449 tropospheric low-pressure anomaly that appears first in December and remains throughout all of DJF  
450 (Figures 6,f,g,i and 10). The generation of this circulation feature was pointed out by previous studies  
451 (Orsolini and Kvamstø, 2009; Garfinkel et al., 2010; Garfinkel et al., 2020), and has been attributed to  
452 an enhanced vertical propagation of Rossby waves into the stratosphere and horizontal downstream of  
453 the cooled Eurasian land mass.

454 Subsampling of the experimental multi-decadal historical hindcasts (ASF-20C EXP) highlighted an  
455 interdecadal variability and non-stationarity of the snow dipole impact, despite the cancelling out of  
456 common boundary forcings such as SSTs in the composite difference. The configuration of our  
457 experiment does not allow to explain this behaviour completely; however, we can address some possible  
458 reasons. A potential influence on the decadal variability of the snow cover impact might be the  
459 precursory climate system state, promoting or counteracting the tendency for the (perturbed) snow  
460 forcing towards a given NAO state.

461 Surprisingly, the positive snow dipole forcing tends to favour a negative NAO signal when the climate  
462 system is “tuned” for a positive winter NAO in ERA20C, for example when high ERA20C Barents-  
463 Kara sea ice extent and La Niña SST conditions prevail (Supplementary Figure S7). This supports the  
464 idea of a clear and strong snow impact when the relative cooling anomaly in Eastern Eurasia is relatively  
465 strong and the climate state is preconditioned to a rather positive NAO-like condition. This might  
466 explain the strong positive NAO anomaly during the early twentieth century Arctic warming in Figure  
467 1d: the period 1920–1940 was characterized by a strong positive mid-tropospheric high anomaly from  
468 Northern Europe to East Siberia (Wegmann et al., 2017a). We find that the 500 hPa anomalies between  
469 high and low snow composites show only a weak to non-existing Ural ridge for the period 1921–1940,  
470 when compared to e.g. 1991–2010 (Supplementary Figure S8). On the contrary, increased snow in an  
471 already snow covered Eastern Eurasia will not provide the same response as the pre-existing anomalies  
472 favoured by other background conditions. Rather, strong non-linearities seem to occur, which is  
473 reasonable given the non-linear thermodynamic and radiative impacts of a deeper snowpack.

474 On that note, we find that the relative magnitude of regional cooling compared to the existing climate  
475 state in our experiments is of crucial importance. In years when the high-low snow dipole anomalies  
476 preceded a negative NAO, the December cooling anomaly over Eastern Eurasia is much stronger than  
477 for the opposite case (Fig. 9). Moreover, we found that in our model experiment a negative snow dipole  
478 forcing leading to a positive NAO signal has a much larger relative impact compared to the positive  
479 snow dipole resulting in a negative NAO signal, which is due to the much stronger changes in surface  
480 forcing that we impose with the negative snow dipole ensemble. Moreover, due to the Eurasian snow

481 climatology, a similar level of snow depth variability in the western domain will have higher impacts  
482 on the tropospheric variability. In our experimental setup, a weak snow depth gradient from west to east  
483 allows for a rather zonal circulation in the following months, with no subsequent stratospheric warming  
484 signal. Distinct model experiments are needed to understand the atmospheric feedbacks of these  
485 configurations better. However, it should be kept in mind for future studies using regression or similar  
486 statistical tools to infer about the impact of Eurasian snow cover.

487 As such, we find that the main driver for the proposed snow-stratosphere linkage is a large relative  
488 impact of the additional snow depth in terms of surface temperatures as well as a strong west-east snow  
489 depth gradient. Generally, our results further highlight the importance behind the land memory effect  
490 discussed by Nakamura et al. (2019), who argue for a delayed impact of snow cover via soil and surface  
491 temperatures.

492 Nevertheless, we are limited in analysing the impact of co-variability in the climate system over the  
493 span of the 110-year period. Additional experiments are needed to investigate the role of climate state  
494 precursors and memory effects influencing the seasonal predictions.

## 495 **5. Summary and Conclusion**

496 Centennial seasonal ensemble hindcasts were used to examine the impact of a realistically increased  
497 November Eurasian west-to-east snow depth gradient on the boreal winter climate evolution. We found  
498 evidence for the manifestation of a negative NAO signal after a strong, positive November west-to-east  
499 snow cover dipole via surface cooling, increased Ural blocking and subsequent stratospheric warming  
500 (although evolution toward a positive NAO state was also observed but less frequently, especially for  
501 NAO extremes). Including 110-years of natural Earth System variability increases the confidence in the  
502 proposed physical mechanisms behind cryospheric drivers of atmospheric variability and decreases the  
503 probability of random co-variability between snow cover and DJF NAO. Our results hence support  
504 previous hypotheses and statistical studies. The absolute surface impact was found to be small in our  
505 experimental setup, with interdecadal variability and ensemble averaging reducing the magnitude of  
506 individual events. We found the impact of our snow forcing to be strongest for climate states that will  
507 allow the snow forcing to exert a strong surface cooling.

508 Future studies need to address the interplay between different Earth System components in coupled  
509 seasonal prediction experiments. How important the background conditions of the climate system are  
510 before the initialization of the forecasts needs to be investigated further. Furthermore, allowing higher  
511 magnitude snow forcing (e.g., perturbing initial land states over a longer range than the neighbouring  
512 10 years as in this study) might result in stronger stratospheric and surface signals.

513

514 **Data availability:**

515 The ERA-20C reanalysis data is publicly available (<https://apps.ecmwf.int/datasets/>). The NAO  
516 reconstruction is publicly available at the Climate Research Unit repository  
517 (<https://crudata.uea.ac.uk/cru/data/nao/>). The ASF-20C dataset is publicly available at the CEDA  
518 Archive (<https://catalogue.ceda.ac.uk/uuid/6e1c3df49f644a0f812818080bed5e45>). The ASF-20C  
519 experiment dataset (created by Bart van den Hurk) can be made available on the ECMWF MARS  
520 system upon request.

521

#### 522 **Author contribution:**

523 MW and YO designed the study. MW analysed the data. AW and BvH provided the data. GL provided  
524 discussion and interpretation of the results. All authors contributed by interpreting the results and  
525 writing the paper.

526

#### 527 **Acknowledgements:**

528 The authors thank Daniel Balting for coding advice and Judah Cohen for fruitful discussions. GL and  
529 MW received funding through BMBF for the topic "Ocean and Cryosphere under climate change" in  
530 the Program "Changing Earth - Sustaining our Future" of the Helmholtz society.

531

#### 532 **Competing Interests:**

533 The authors declare no competing interests.

#### 534 **References**

535 Athanasiadis, P. J., Bellucci, A., Scaife, A. A., Hermanson, L., Materia, S., Sanna, A., Borrelli, A.,  
536 MacLachlan, C., and Gualdi, S.: A multisystem view of wintertime nao seasonal predictions,  
537 *Journal of Climate*, 30, 1461–1475, <https://doi.org/10.1175/JCLI-D-16-0153>, 2017.

538 Baker, L. H., Shaffrey, L. C., Sutton, R. T., Weisheimer, A., and Scaife, A. A.: An intercomparison of  
539 skill and overconfidence/underconfidence of the wintertime north atlantic oscillation in  
540 multimodel seasonal forecasts, *Geophysical Research Letters*, 45, 7808–7817,  
541 <https://doi.org/https://doi.org/10.1029/2018GL078838>, 2018.

542 Blunden, J., and Boyer, T.: State of the Climate in 2020, *Bulletin of the American Meteorological*  
543 *Society*, 102, S1-S475, 2021.

544 Cohen, J., Barlow, M., Kushner, P. J., and Saito, K.: Stratosphere–troposphere coupling and links with  
545 eurasian land surface variability, *Journal of Climate*, 20, 5335–5343,  
546 <https://doi.org/10.1175/2007JCLI1725.1>, 2007.

547 Cohen, J., and Entekhabi, D.: Eurasian snow cover variability and northern hemisphere climate  
548 predictability, *Geophysical Research Letters*, 26, 345–348,  
549 <https://doi.org/https://doi.org/10.1029/1998GL900321>, 1999.

550 Cohen, J., and Jones, J.: A new index for more accurate winter predictions, *Geophysical Research*  
551 *Letters*, 38, <https://doi.org/https://doi.org/10.1029/2011GL049626>, 2011.

552 Cohen, J., and Rind, D.: The effect of snow cover on the climate, *Journal of Climate*, 4, 689–706,  
553 [https://doi.org/10.1175/1520-0442\(1991\)004<0689:TEOSCO>2.0.CO;2](https://doi.org/10.1175/1520-0442(1991)004<0689:TEOSCO>2.0.CO;2), 1991.

554 Cohen, J., Screen, J. A., Furtado, J. C., Barlow, M., Whittleston, D., Coumou, D., Francis, J., Dethloff,  
555 K., Entekhabi, D., Overland, J., and Jones, J.: Recent Arctic amplification and extreme mid-  
556 latitude weather, *Nature Geoscience*, 7, 627–637, <https://doi.org/10.1038/ngeo2234>, 2014.

557 Deser, C., Hurrell, J. W., and Phillips, A. S.: The role of the north atlantic oscillation in european climate  
558 projections, *Climate Dynamics*, 49, 3141–3157, <https://doi.org/10.1007/s00382-016-3502-z>,  
559 2017.

560 Cohen, J., Agel, L., Barlow, M., Garfinkel, C. I., and White, I.: Linking Arctic variability and change  
561 with extreme winter weather in the United States. *Science*, 373, 1116-1121, 2021.

562 Dirmeyer, P. A., Kumar, S., Fennessy, M. J., Altshuler, E. L., DelSole, T., Guo, Z., Cash, B. A., and  
563 Straus, D.: Model estimates of land-driven predictability in a changing climate from cesm4,  
564 *Journal of Climate*, 26, 8495–8512, <https://doi.org/10.1175/JCLI-D-13-00029.1>, 2013.

565 Diro, G. T., and Lin, H.: Subseasonal Forecast Skill of Snow Water Equivalent and Its Link with  
566 Temperature in Selected SubX Models. *Weather and Forecasting*, 35(1), 273-284, 2020.

567 Douville, H., Peings, Y., and Saint-Martin, D.: Snow-(N)AO relationship revisited over the whole  
568 twentieth century, *Geophysical Research Letters*, 44, 569–577,  
569 <https://doi.org/https://doi.org/10.1002/2016GL071584>, 2017.

570 Dunstone, N., Smith, D., Scaife, A., Hermanson, L., Eade, R., Robinson, N., Andrews, M., and Knight,  
571 J.: Skilful predictions of the winter North Atlantic Oscillation one year ahead, *Nature*  
572 *Geoscience*, 9, 809–814, <https://doi.org/10.1038/ngeo2824>, 2016.

573 Dutra, E., Schär, C., Viterbo, P., and Miranda, P. M. A.: Land-atmosphere coupling associated with  
574 snow cover, *Geophysical Research Letters*, 38,  
575 <https://doi.org/https://doi.org/10.1029/2011GL048435>, 2011.

576 Fletcher, C. G., Hardiman, S. C., Kushner, P. J., and Cohen, J.: The dynamical response to snow cover  
577 perturbations in a large ensemble of atmospheric gcm integrations, *Journal of Climate*, 22,  
578 1208–1222, <https://doi.org/10.1175/2008JCLI2505.1>, 2009.

579 Furtado, J. C., Cohen, J. L., Butler, A. H., Riddle, E. E., and Kumar, A.: Eurasian snow cover variability  
580 and links to winter climate in the CMIP5 models, *Climate Dynamics*, 45, 2591–2605,  
581 <https://doi.org/10.1007/s00382-015-2494-4>, 2015.

582 Furtado, J. C., Cohen, J. L., and Tziperman, E.: The combined influences of autumnal snow and sea ice  
583 on Northern Hemisphere winters, *Geophysical Research Letters*, 43, 3478–3485,  
584 <https://doi.org/https://doi.org/10.1002/2016GL068108>, 2016.

585 Garfinkel, C. I., Hartmann, D. L., and Sassi, F.: Tropospheric precursors of anomalous northern  
586 hemisphere stratospheric polar vortices, *Journal of Climate*, 23, 3282–3299,  
587 <https://doi.org/10.1175/2010JCLI3010.1>, 2010.

588 Garfinkel, C. I., Schwartz, C., White, I. P., and Rao, J.: Predictability of the early winter Arctic  
589 oscillation from autumn Eurasian snowcover in subseasonal forecast models, *Climate*  
590 *Dynamics*, 55, 961–974, <https://doi.org/10.1007/s00382-020-05305-3>, 2020.

591 Gastineau, G., García-Serrano, J., and Frankignoul, C.: The influence of autumnal eurasian snow cover  
592 on climate and its link with arctic sea ice cover, *Journal of Climate*, 30, 7599–7619,  
593 <https://doi.org/10.1175/JCLI-D-16-0623.1>, 2017.

594 Ghatak, D., Frei, A., Gong, G., Stroeve, J., and Robinson, D.: On the emergence of an Arctic  
595 amplification signal in terrestrial Arctic snow extent, *Journal of Geophysical Research:*  
596 *Atmospheres*, 115, <https://doi.org/https://doi.org/10.1029/2010JD014007>, 2010.

597 Gong, G., Entekhabi, D., and Cohen, J.: Modeled northern hemisphere winter climate response to  
598 realistic siberian snow anomalies, *Journal of Climate*, 16, 3917–3931,  
599 [https://doi.org/10.1175/1520-0442\(2003\)016<3917:MNHWCR>2.0.CO;2](https://doi.org/10.1175/1520-0442(2003)016<3917:MNHWCR>2.0.CO;2), 2003.

600 Han, S., and Sun, J.: Impacts of autumnal eurasian snow cover on predominant modes of boreal winter  
601 surface air temperature over eurasia, *Journal of Geophysical Research: Atmospheres*, 123,  
602 10,076-10,091, <https://doi.org/https://doi.org/10.1029/2018JD028443>, 2018.

603 Hardiman, S. C., Kushner, P. J., and Cohen, J.: Investigating the ability of general circulation models  
604 to capture the effects of Eurasian snow cover on winter climate, *Journal of Geophysical*  
605 *Research: Atmospheres*, 113, <https://doi.org/https://doi.org/10.1029/2008JD010623>, 2008.

606 Henderson, G. R., Peings, Y., Furtado, J. C., and Kushner, P. J.: Snow–atmosphere coupling in the  
607 Northern Hemisphere, *Nature Climate Change*, 8, 954–963, [https://doi.org/10.1038/s41558-](https://doi.org/10.1038/s41558-018-0295-6)  
608 [018-0295-6](https://doi.org/10.1038/s41558-018-0295-6), 2018.

609 Hurrell, J. W., and Deser, C.: North atlantic climate variability: The role of the north atlantic oscillation,  
610 *Journal of Marine Systems*, 79, 231–244, <https://doi.org/10.1016/j.jmarsys.2009.11.002>, 2010.

611 Jones, P. D., Jonsson, T., and Wheeler, D.: Extension to the North Atlantic Oscillation using early  
612 instrumental pressure observations from Gibraltar and south-west Iceland. *International*  
613 *Journal of climatology*, 17, 1433-1450, 1997

614 Kang, D., Lee, M.-I., Im, J., Kim, D., Kim, H.-M., Kang, H.-S., Schubert, S. D., Arribas, A., and  
615 MacLachlan, C.: Prediction of the Arctic Oscillation in boreal winter by dynamical seasonal  
616 forecasting systems, *Geophysical Research Letters*, 41, 3577–3585,  
617 <https://doi.org/https://doi.org/10.1002/2014GL060011>, 2014.

618 Koster, R. D., Mahanama, S. P., Yamada, T. J., Balsamo, G., Berg, A. A., Boisserie, M., Dirmeyer, P.  
619 A., Doblas-Reyes, F. J., Drewitt, G., Gordon, C. T., Guo, Z., Jeong, J.-H., Lee, W.-S., Li, Z.,  
620 Luo, L., Malyshev, S., Merryfield, W. J., Seneviratne, S. I., Stanelle, T., Van den Hurk, B.,  
621 Vitart, F. and Wood, E. F.: The second phase of the Global Land–Atmosphere Coupling  
622 Experiment: Soil moisture contributions to subseasonal forecast skill. *Journal of*  
623 *Hydrometeorology*, 12(5), 805-822, 2011.

624 Kretschmer, M., Coumou, D., Agel, L., Barlow, M., Tziperman, E., and Cohen, J.: More-persistent  
625 weak stratospheric polar vortex states linked to cold extremes, *Bulletin of the American*  
626 *Meteorological Society*, 99, 49–60. <https://doi.org/10.1175/BAMS-D-16-0259.1>, 2018.

627 Li, F., Orsolini, Y. J., Keenlyside, N., Shen, M.-L., Counillon, F., and Wang, Y. G.: Impact of snow  
628 initialization in subseasonal-to-seasonal winter forecasts with the norwegian climate prediction  
629 model, *Journal of Geophysical Research: Atmospheres*, 124, 10033–10048,  
630 <https://doi.org/https://doi.org/10.1029/2019JD030903>, 2019.

631 Lü, Z., Li, F., Orsolini, Y., Gao, Y., He, S.: Understanding of European Cold Extremes, Sudden  
632 Stratospheric Warming, and Siberian Snow Accumulation in the Winter of 2017/18, *Journal of*  
633 *Climate*, Vol. 33. s.527-545, 2020.

634 Meehl, G. A., Richter, J. H., Teng, H., Capotondi, A., Cobb, K., Doblas-Reyes, F., Donat, M. G.,  
635 England, M. H., Fyfe, J. C., Han, W., Kim, H., Kirtman, B. P., Kushnir Y., Lovenduski, N. S.,  
636 Mann, M. E., Merryfield, W. J., Nieves, V., Pegion, K., Rosenbloom, N., Sanchez, S. C.,  
637 Scaife, A. A., Smith, D., Subramanian, A. C., Sun, L., Thompson, D., Ummenhofer, C. C. and  
638 Xie, S.-P.: Initialized Earth System prediction from subseasonal to decadal timescales. *Nat*  
639 *Rev Earth Environ* 2, 340–357. <https://doi.org/10.1038/s43017-021-00155-x>, 2021.

640 Molteni, F., Stockdale, T., Alonso-Balmaseda, M., Balsamo, G., Buizza, R., Ferranti, L., Magnusson,  
641 L., Mogensen, K., Palmer, T. N., and Vitart, F.: The new ECMWF seasonal forecast system  
642 (System 4). ECMWF Technical Memorandum #656, 2011.



643 Moore, G. W. K., and Renfrew, I. A.: Cold European winters: Interplay between the NAO and the East  
644 Atlantic mode, *Atmospheric Science Letters*, 13, 1–8.  
645 <https://doi.org/https://doi.org/10.1002/asl.356>, 2012.

646 Nakamura, T., Yamazaki, K., Sato, T., and Ukita, J.: Memory effects of Eurasian land processes cause  
647 enhanced cooling in response to sea ice loss, *Nature Communications*, 10, 5111.  
648 <https://doi.org/10.1038/s41467-019-13124-2>, 2019.

649 O’Reilly, C. H., Heatley, J., MacLeod, D., Weisheimer, A., Palmer, T. N., Schaller, N., and Woollings,  
650 T.: Variability in seasonal forecast skill of Northern Hemisphere winters over the twentieth  
651 century, *Geophysical Research Letters*, 44, 5729–5738,  
652 <https://doi.org/https://doi.org/10.1002/2017GL073736>, 2017.

653 O’Reilly, C. H., Weisheimer, A., MacLeod, D., Befort, D. J., and Palmer, T.: Assessing the robustness  
654 of multidecadal variability in Northern Hemisphere wintertime seasonal forecast skill,  
655 *Quarterly Journal of the Royal Meteorological Society*, 146, 4055–4066,  
656 <https://doi.org/https://doi.org/10.1002/qj.3890>, 2020.

657 Orsolini, Y. J., Senan, R., Balsamo, G., Doblas-Reyes, F. J., Vitart, F., Weisheimer, A., Carrasco, A.,  
658 and Benestad, R. E.: Impact of snow initialization on sub-seasonal forecasts, *Climate*  
659 *Dynamics*, 41, 1969–1982, <https://doi.org/10.1007/s00382-013-1782-0>, 2013.

660 Orsolini, Y. J., Senan, R., Vitart, F., Balsamo, G., Weisheimer, A., and Doblas-Reyes, F. J.: Influence  
661 of the Eurasian snow on the negative North Atlantic Oscillation in subseasonal forecasts of the  
662 cold winter 2009/2010, *Climate Dynamics*, 47, 1325–1334, [https://doi.org/10.1007/s00382-](https://doi.org/10.1007/s00382-015-2903-8)  
663 [015-2903-8](https://doi.org/10.1007/s00382-015-2903-8), 2016.

664 Parker, T., Woollings, T., Weisheimer, A., O’Reilly, C., Baker, L., and Shaffrey, L.: Seasonal  
665 predictability of the winter north atlantic oscillation from a jet stream perspective, *Geophysical*  
666 *Research Letters*, 46, 10159–10167, <https://doi.org/https://doi.org/10.1029/2019GL084402>,  
667 2019.

668 Peings, Y.: Ural blocking as a driver of early-winter stratospheric warmings, *Geophysical Research*  
669 *Letters*, 46, 5460–5468, <https://doi.org/https://doi.org/10.1029/2019GL082097>, 2019.

670 Peings, Y., Brun, E., Mauvais, V., and Douville, H.: How stationary is the relationship between Siberian  
671 snow and Arctic Oscillation over the 20th century?, *Geophysical Research Letters*, 40, 183–  
672 188, <https://doi.org/https://doi.org/10.1029/2012GL054083>, 2013.

673 Peings, Y., Douville, H., Colin, J., Martin, D. S., and Magnusdottir, G.: Snow–(N)ao teleconnection  
674 and its modulation by the quasi-biennial oscillation, *Journal of Climate*, 30, 10211–10235,  
675 <https://doi.org/10.1175/JCLI-D-17-0041.1>, 2017.

676 Peings, Y., Saint-Martin, D., and Douville, H.: A numerical sensitivity study of the influence of siberian  
677 snow on the northern annular mode, *Journal of Climate*, 25, 592–607,  
678 <https://doi.org/10.1175/JCLI-D-11-00038.1>, 2012.

679 Polyakov, I. V., Bekryaev, R. V., Alekseev, G. V., Bhatt, U. S., Colony, R. L., Johnson, M. A.,  
680 Maskshtas, A. P. and Walsh, D.: Variability and trends of air temperature and pressure in the  
681 maritime Arctic, 1875–2000. *Journal of Climate*, 16(12), 2067-2077, 2003

682 Portal, A., Ruggieri, P., Palmeiro, F. M., García-Serrano, J., Domeisen, D. I., & Gualdi, S.: Seasonal  
683 prediction of the boreal winter stratosphere, *Climate Dynamics*, 1-22, 2021.

684 Santolaria-Otín, M., García-Serrano, J., Ménégos, M., and Bech, J.: On the observed connection  
685 between Arctic sea ice and Eurasian snow in relation to the winter North Atlantic Oscillation,  
686 *Environmental Research Letters*, 15, 124010, <https://doi.org/10.1088/1748-9326/abad57>, 2021.

687 Santolaria-Otín, M., and Zolina, O.: Evaluation of snow cover and snow water equivalent in the  
688 continental Arctic in CMIP5 models, *Climate Dynamics*, 55, 2993–3016,  
689 <https://doi.org/10.1007/s00382-020-05434-9>, 2020.

690 Scaife, A. A., Arribas, A., Blockley, E., Brookshaw, A., Clark, R. T., Dunstone, N., Eade, R., Fereday,  
691 D., Folland, C. K., Gordon, M., Hermanson, L., Knight, J. R., Lea, D. J., MacLachlan, C.,  
692 Maidens, A., Martin, M., Peterson, A. K., Smith, D., Vellinga, M., Wallace, E., Waters, J. and  
693 Williams, A.: Skillful long-range prediction of European and North American winters,  
694 *Geophysical Research Letters*, 41, 2514–2519,  
695 <https://doi.org/https://doi.org/10.1002/2014GL059637>, 2014.

696 Scaife, A. A., Karpechko, A. Y., Baldwin, M. P., Brookshaw, A., Butler, A. H., Eade, R., Gordon, M.,  
697 MacLachlan, C., Martin, N., Dunstone, N., and Smith, D.: Seasonal winter forecasts and the  
698 stratosphere, *Atmospheric Science Letters*, 17, 51–56,  
699 <https://doi.org/https://doi.org/10.1002/asl.598>, 2016.

700 Smith, D. M., Scaife, A. A., Eade, R., and Knight, J. R.: Seasonal to decadal prediction of the winter  
701 North Atlantic Oscillation: Emerging capability and future prospects, *Quarterly Journal of the*  
702 *Royal Meteorological Society*, 142, 611–617, <https://doi.org/https://doi.org/10.1002/qj.2479>,  
703 2016.

704 Song, L., & Wu, R., 2019: Intraseasonal snow cover variations over western Siberia and associated  
705 atmospheric processes, *Journal of Geophysical Research: Atmospheres*, 124, 8994–  
706 9010. Thackeray, C. W., Derksen, C., Fletcher, C. G., and Hall, A.: Snow and climate:  
707 Feedbacks, drivers, and indices of change, *Current Climate Change Reports*, 5, 322–333,  
708 <https://doi.org/10.1007/s40641-019-00143-w>, 2019.

709 Thompson, D. W. J., and Wallace, J. M.: The Arctic oscillation signature in the wintertime geopotential  
710 height and temperature fields, *Geophysical Research Letters*, 25, 1297–1300,  
711 <https://doi.org/10.1029/98GL00950> , 1998.

712 Tian, B., and Fan, K.: A skillful prediction model for winter nao based on atlantic sea surface  
713 temperature and eurasian snow cover, *Weather and Forecasting*, 30, 197–205,  
714 <https://doi.org/10.1175/WAF-D-14-00100.1>, 2015.

715 Tyrrell, N. L., Karpechko, A. Y., and Räisänen, P.: The influence of eurasian snow extent on the  
716 northern extratropical stratosphere in a qbo resolving model, *Journal of Geophysical Research:*  
717 *Atmospheres*, 123, 315–328, <https://doi.org/https://doi.org/10.1002/2017JD027378>, 2018.

718 Tyrrell, N. L., Karpechko, A. Y., Uotila, P., and Vihma, T.: Atmospheric circulation response to  
719 anomalous siberian forcing in october 2016 and its long-range predictability, *Geophysical*  
720 *Research Letters*, 46, 2800–2810, <https://doi.org/https://doi.org/10.1029/2018GL081580> ,  
721 2019.

722 van den Hurk, B., Kim, H., Krinner, G., Seneviratne, S. I., Derksen, C., Oki, T., Douville, H., Colin, J.,  
723 Ducharne, A., Cheruy, F., Viovy, N., Puma, M. J., Wada, Y., Li, W., Jia, B., Alessandri, A.,  
724 Lawrence, D. M., Weedon, G. P., Ellis, R., Hagemann, S., Mao, J., Flanner, M. G., Zampieri,  
725 M., Materia, S., Law, R. M., and Sheffield, J.: Ls3mip (V1. 0) contribution to cmip6: The land  
726 surface, snow and soil moisture model intercomparison project – aims, setup and expected  
727 outcome, *Geoscientific Model Development*, 9, 2809–2832, [https://doi.org/10.5194/gmd-9-](https://doi.org/10.5194/gmd-9-2809-2016)  
728 [2809-2016](https://doi.org/10.5194/gmd-9-2809-2016) , 2016.

729 Vavrus, S.: The role of terrestrial snow cover in the climate system, *Climate Dynamics*, 29, 73–88,  
730 <https://doi.org/10.1007/s00382-007-0226-0>, 2007.

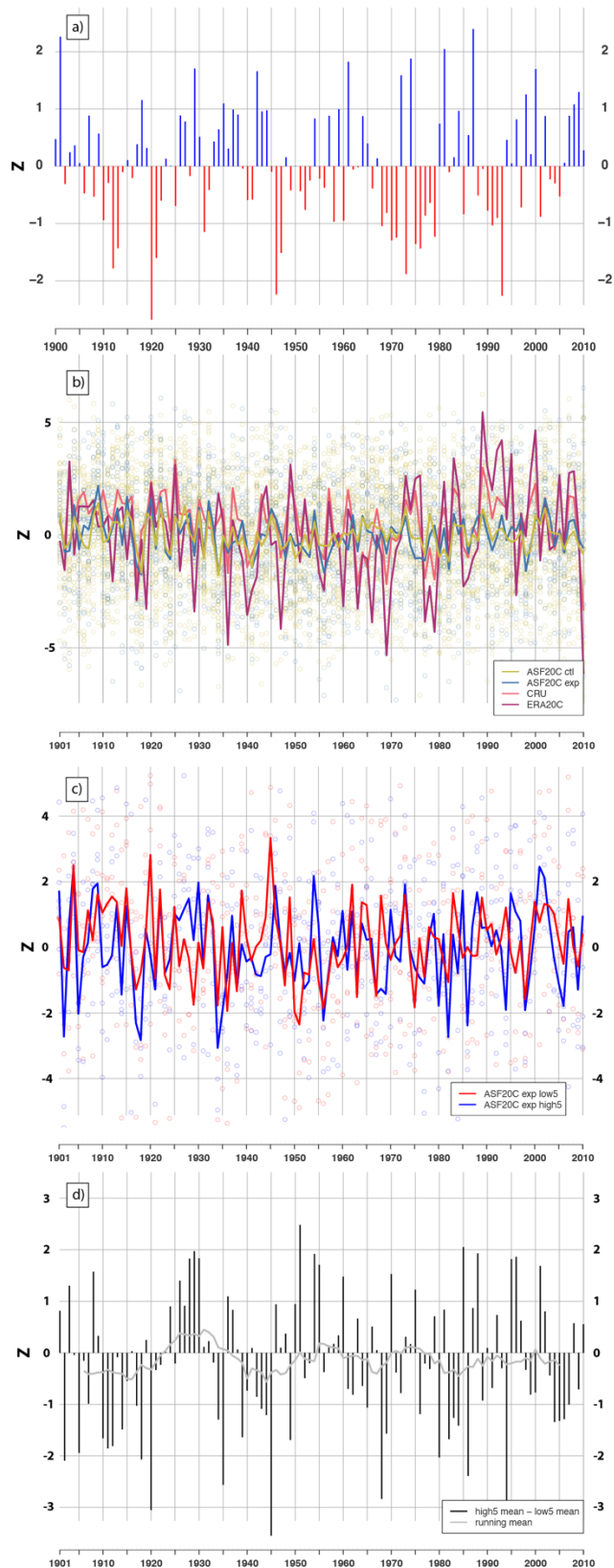
731 Wang, L., Ting, M., and Kushner, P. J.: A robust empirical seasonal prediction of winter NAO and  
732 surface climate, *Scientific Reports*, 7, 279, <https://doi.org/10.1038/s41598-017-00353-y> , 2017.

733 Wanner, H., Brönnimann, S., Casty, C., Gyalistras, D., Luterbacher, J., Schmutz, C., Stephenson, D. B.,  
734 and Xoplaki, E.: North atlantic oscillation – concepts and studies, *Surveys in Geophysics*, 22,  
735 321–381, <https://doi.org/10.1023/A:1014217317898>, 2001.

736 Wegmann, M., Orsolini, Y., Vázquez, M., Gimeno, L., Nieto, R., Bulygina, O., Jaiser, R., Handorf, D.,  
737 Rinke, A., Dethloff, K., Sterin, A., and Brönnimann, S.: Arctic moisture source for Eurasian  
738 snow cover variations in autumn, *Environmental Research Letters*, 10, 054015,  
739 <https://doi.org/10.1088/1748-9326/10/5/054015>, 2015.

740 Wegmann, M., Brönnimann, S., and Compo, G. P.: Tropospheric circulation during the early  
741 twentieth century Arctic warming. *Climate dynamics*, 48, 2405-2418, 2017a.

- 742 Wegmann, M., Orsolini, Y., Dutra, E., Bulygina, O., Sterin, A., & Brönnimann, S.: Eurasian snow  
743 depth in long-term climate reanalyses. *The Cryosphere*, 11, 923-935, 2017b
- 744 Wegmann, M., Rohrer, M., Santolaria-Otín, M., and Lohmann, G.: Eurasian autumn snow link to winter  
745 North Atlantic Oscillation is strongest for Arctic warming periods, *Earth System Dynamics*, 11,  
746 509–524, <https://doi.org/https://doi.org/10.5194/esd-11-509-2020>, 2020.
- 747 Weisheimer, A., Befort, D. J., MacLeod, D., Palmer, T., O'Reilly, C., and Strømmen, K.: Seasonal  
748 forecasts of the twentieth century, *Bulletin of the American Meteorological Society*, 101,  
749 E1413–E1426, <https://doi.org/10.1175/BAMS-D-19-0019.1>, 2020.
- 750 Weisheimer, A., Decremmer, D., MacLeod, D., O'Reilly, C., Stockdale, T. N., Johnson, S., and Palmer,  
751 T. N.: How confident are predictability estimates of the winter North Atlantic Oscillation?,  
752 *Quarterly Journal of the Royal Meteorological Society*, 145, 140–159,  
753 <https://doi.org/https://doi.org/10.1002/qj.3446>, 2019.
- 754 Weisheimer, A., Schaller, N., O'Reilly, C., MacLeod, D. A., and Palmer, T.: Atmospheric seasonal  
755 forecasts of the twentieth century: Multi-decadal variability in predictive skill of the winter  
756 North Atlantic Oscillation (Nao) and their potential value for extreme event attribution,  
757 *Quarterly Journal of the Royal Meteorological Society*, 143, 917–926,  
758 <https://doi.org/https://doi.org/10.1002/qj.2976>, 2017.
- 759 White, R. H., Battisti, D. S., & Roe, G. H.: Mongolian Mountains Matter Most: Impacts of the Latitude  
760 and Height of Asian Orography on Pacific Wintertime Atmospheric Circulation, *Journal of*  
761 *Climate*, 30, 4065-4082, 2017.
- 762 Zhang, R., Sun, C., Zhang, R., Li, W., and Zuo, J.: Role of Eurasian snow cover in linking winter-spring  
763 Eurasian coldness to the autumn arctic sea ice retreat, *Journal of Geophysical Research:*  
764 *Atmospheres*, 124, 9205–9221, <https://doi.org/https://doi.org/10.1029/2019JD030339>, 2019.

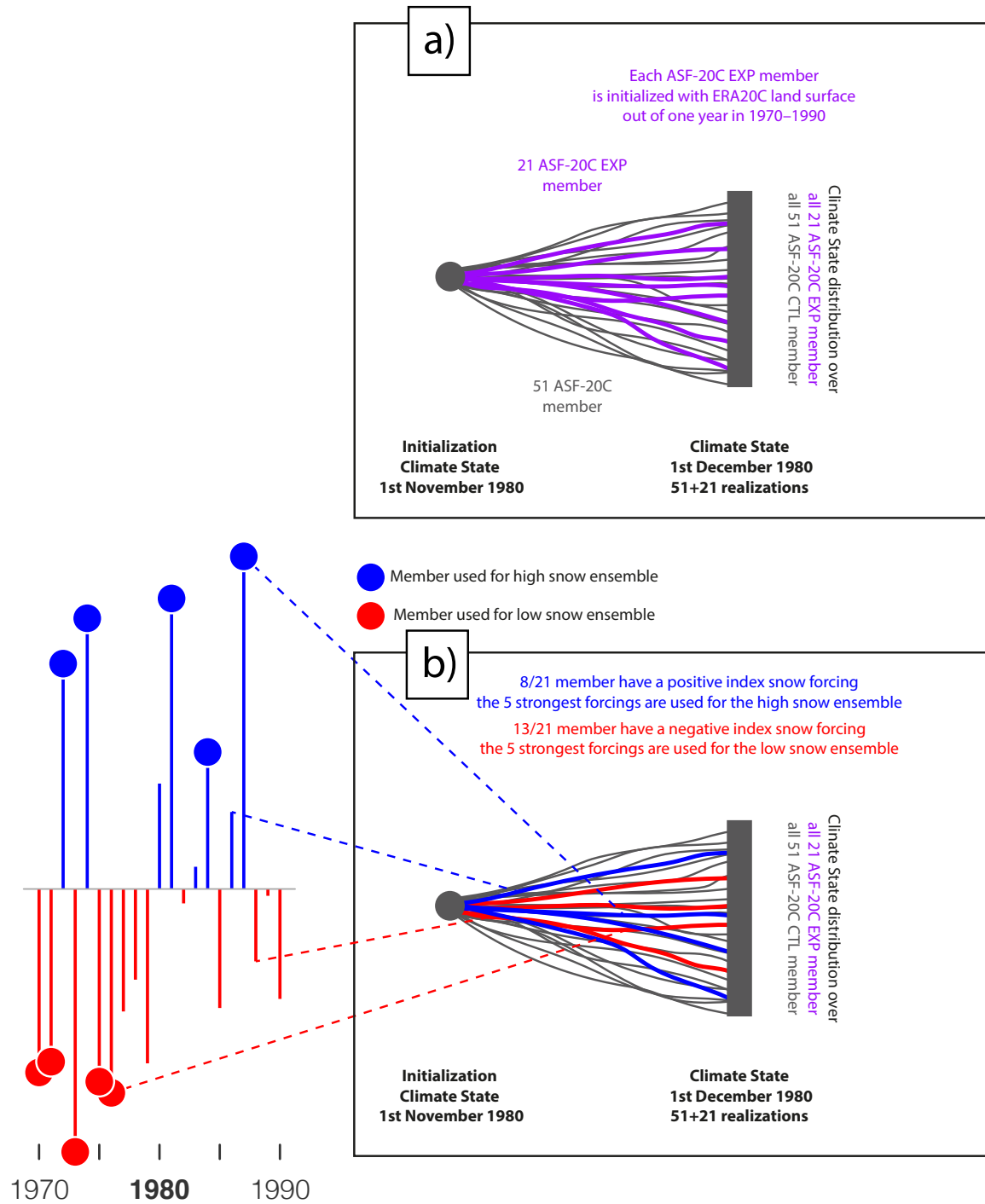


765

766 *Figure 1: a) Normalized 1st of November Eurasian snow dipole index for the period 1900–2010 as*  
 767 *derived from ERA20C. b) Normalized DJF NAO index in the CRU station-based reconstruction,*  
 768 *ERA20C EOF-based index, ASF-20C CTL and ASF-20C EXP EOF-based index. Hollow points*

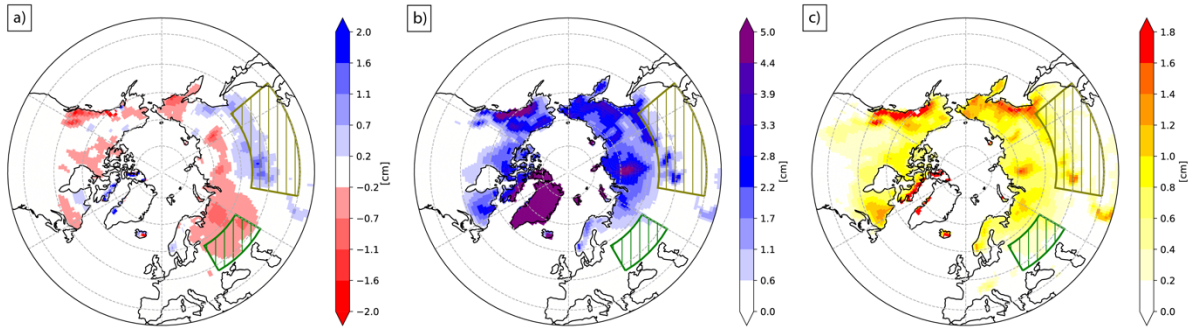
769 *represent individual members, solid lines represent ensemble means or observational products. c) 5-*  
770 *member DJF NAO forecasts for the high- and low-dipole members within ASF-20C EXP. Hollow points*  
771 *represent individual members, solid lines represent ensemble means. d) NAO DJF state difference and*  
772 *its 11-year running mean between the ASF-20C EXP high- and low-dipole ensemble mean in panel b*  
773 *(51(18) cases of positive (+1 SD) NAO response, 59 (29) cases of negative (-1 SD) NAO response). For*  
774 *2 SD exceedance, the number of cases is 2 vs 9.*

775



776

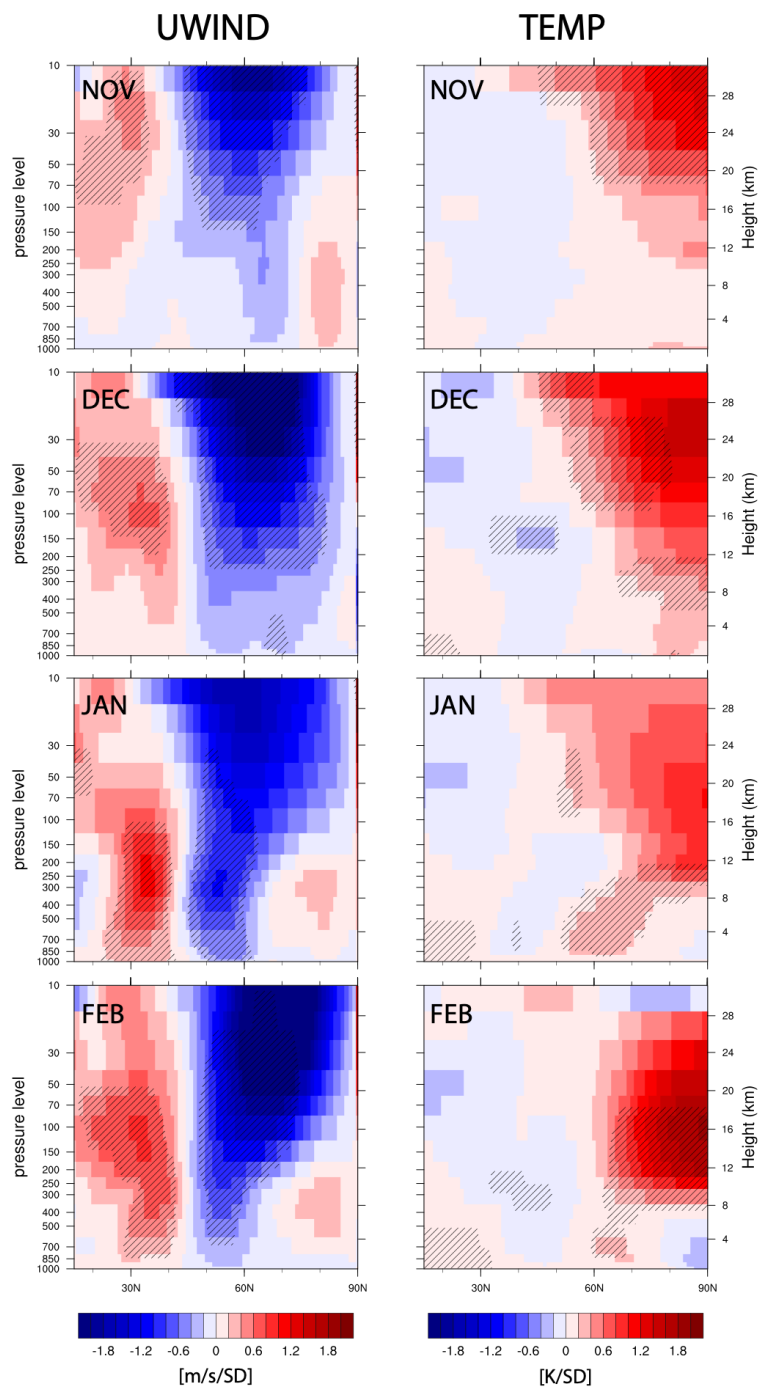
777 *Figure 2: As an example, the schematic for a) the 1980 1st of November ASF-20C EXP initialization*  
 778 *and the consequent sampling of the 21 ensemble members into the high and low snow dipole ensembles.*  
 779 *For the 1st of November initialization, ASF-20C EXP members are initialized by land surface*  
 780 *conditions of the 21 surrounding 1st of November dates, in this case 1970–1990, b) Out of these 21*  
 781 *members, we sample individual members based on their ranking in the snow index. The five members*  
 782 *with the most positive snow index constitute the high snow ensemble and vice versa for the low snow*  
 783 *ensemble.*



784  
 785  
 786  
 787  
 788  
 789

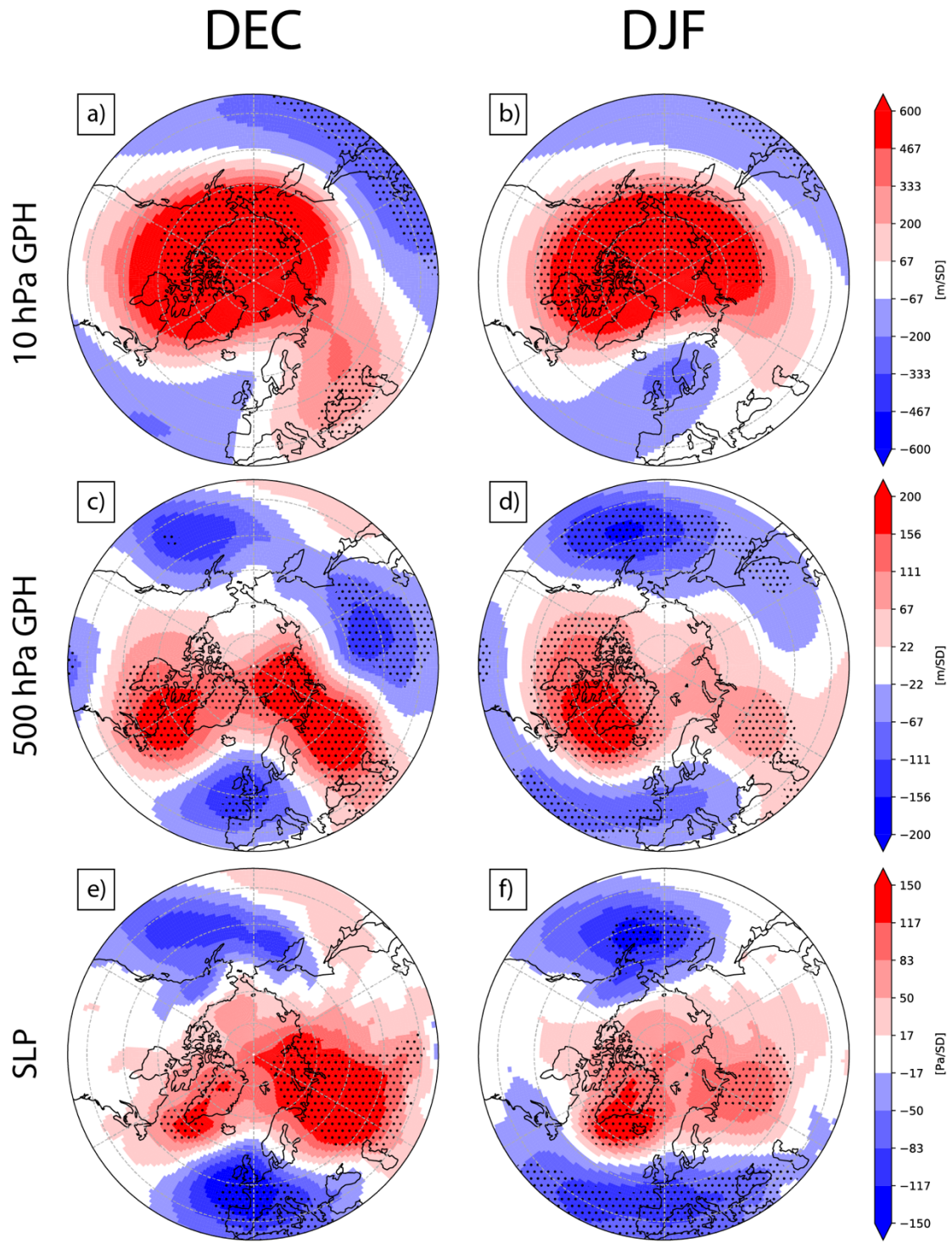
Figure 3: a) Average (1900–2010) 1<sup>st</sup> of November snow depth difference between the high-dipole and low-dipole ensemble. b) Average (1900–2010) 1<sup>st</sup> of November snow depth. c) Average (1900–2010) 1<sup>st</sup> of November snow depth standard deviation. Hatched in green (olive) is the western (eastern) domain of the snow index. All 3 plots are based on ERA20C.





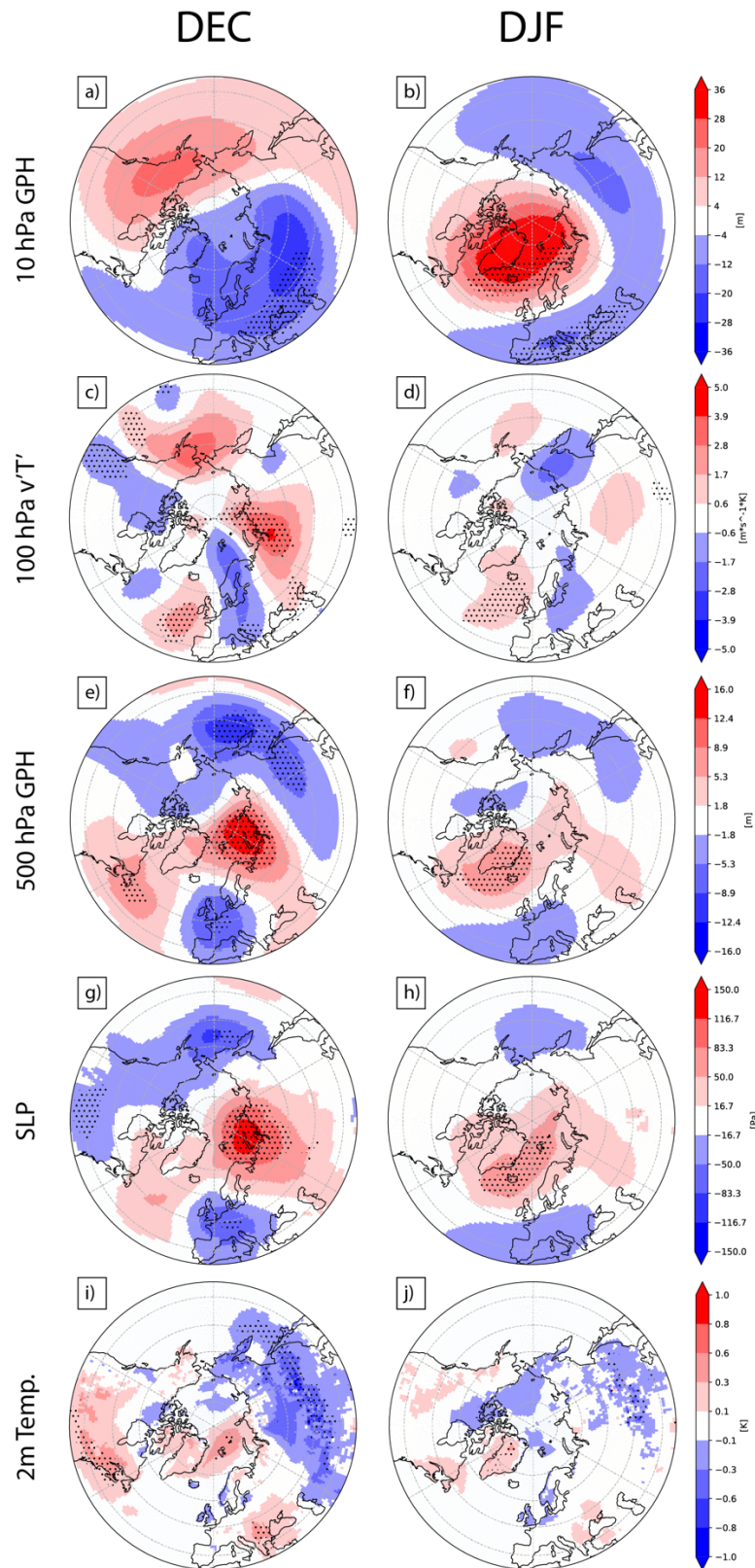
791

792 *Figure 4: Zonal-mean meridional cross-section of ERA20C anomalies in temperature and zonal wind*  
 793 *regressed onto the snow dipole index in November from ERA20C covering 1901–2010 for November,*  
 794 *December, January and February. Shading indicates 95% significance level.*



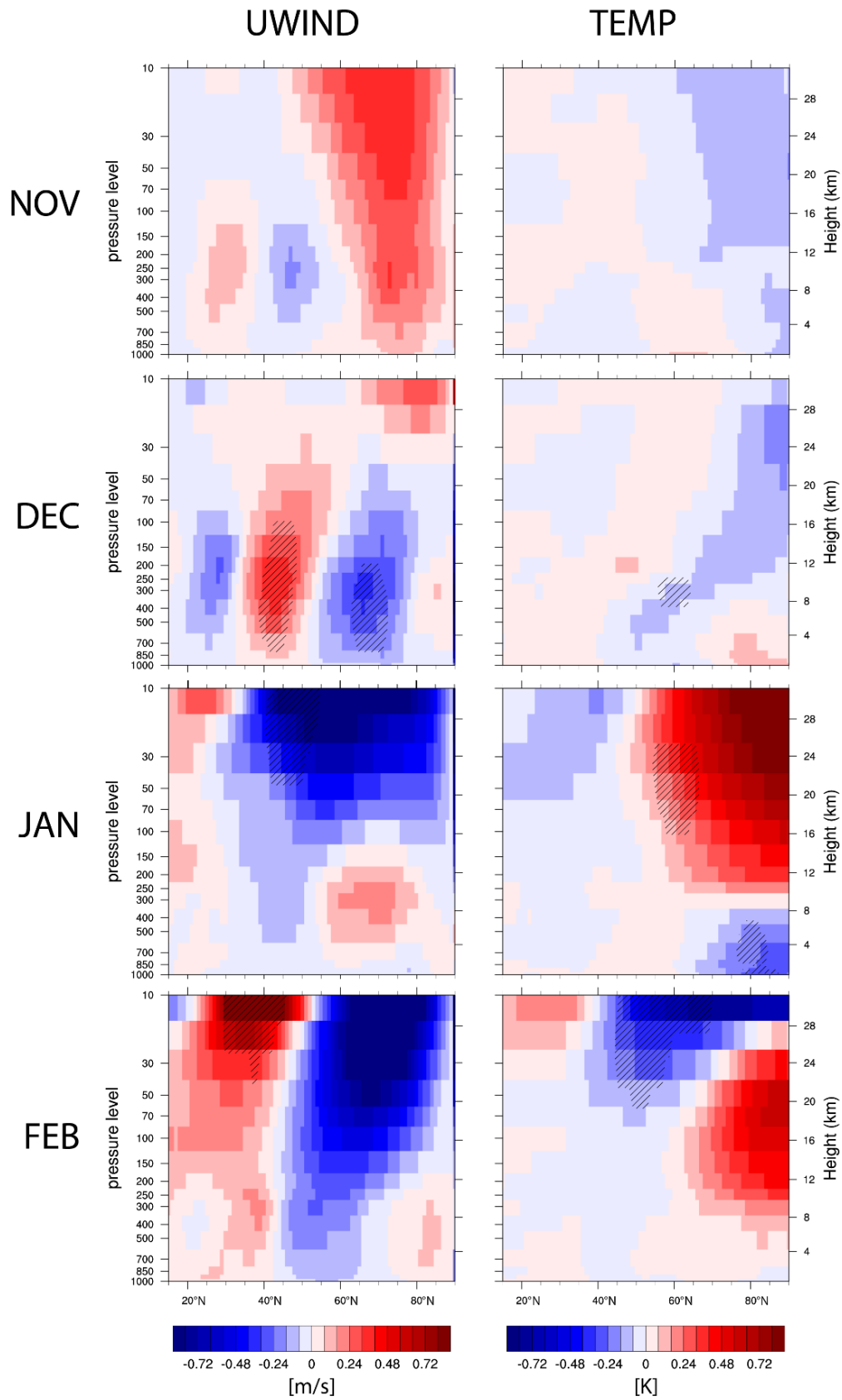
795

796 *Figure 5: ERA20C anomalies of a&b) 10 hPa geopotential heights, c&d) 500 hPa geopotential heights*  
 797 *and e&f) Sea Level Pressure regressed onto the snow dipole index in November from ERA20C covering*  
 798 *1901–2010 for December and DJF mean. Shading indicates 95% significance level. For monthly*  
 799 *anomalies see Supplementary Figure S9.*



800

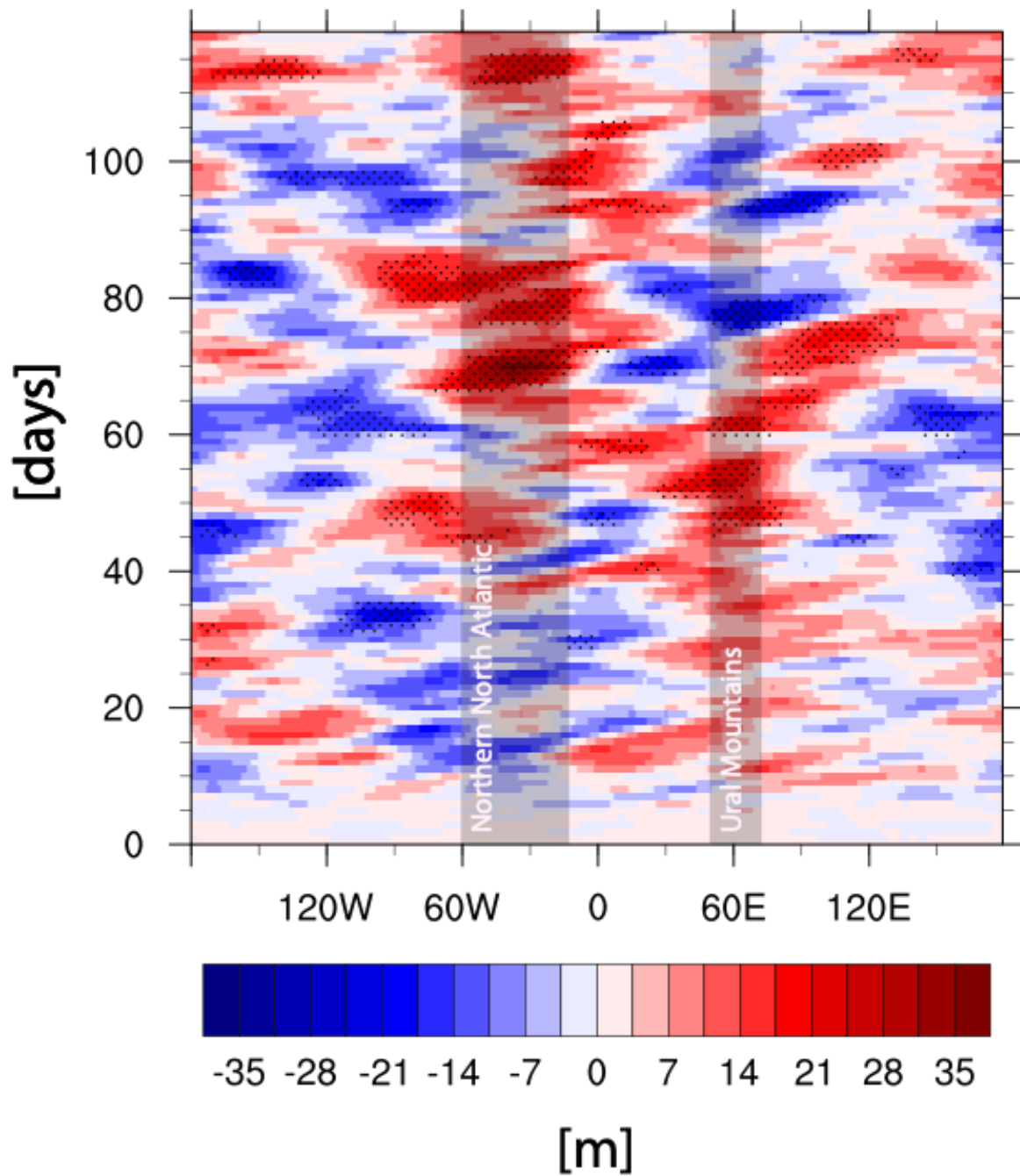
801 *Figure 6: Averaged anomalies 1901-2010 between high-dipole and low-dipole ASF-20C EXP ensemble*  
 802 *means for December (a,c,e,g,i), and DJF (b,d,f,h,j): a&b) 10 hPa geopotential heights, c&d) 100 hPa*  
 803 *meridional eddy heat flux, e&f) 500 hPa geopotential heights, g&h) sea level pressure and i&j) 2m*  
 804 *temperature. Stippled areas represent 90% significance. For monthly anomalies see Supplementary*  
 805 *Figure S10.*



806

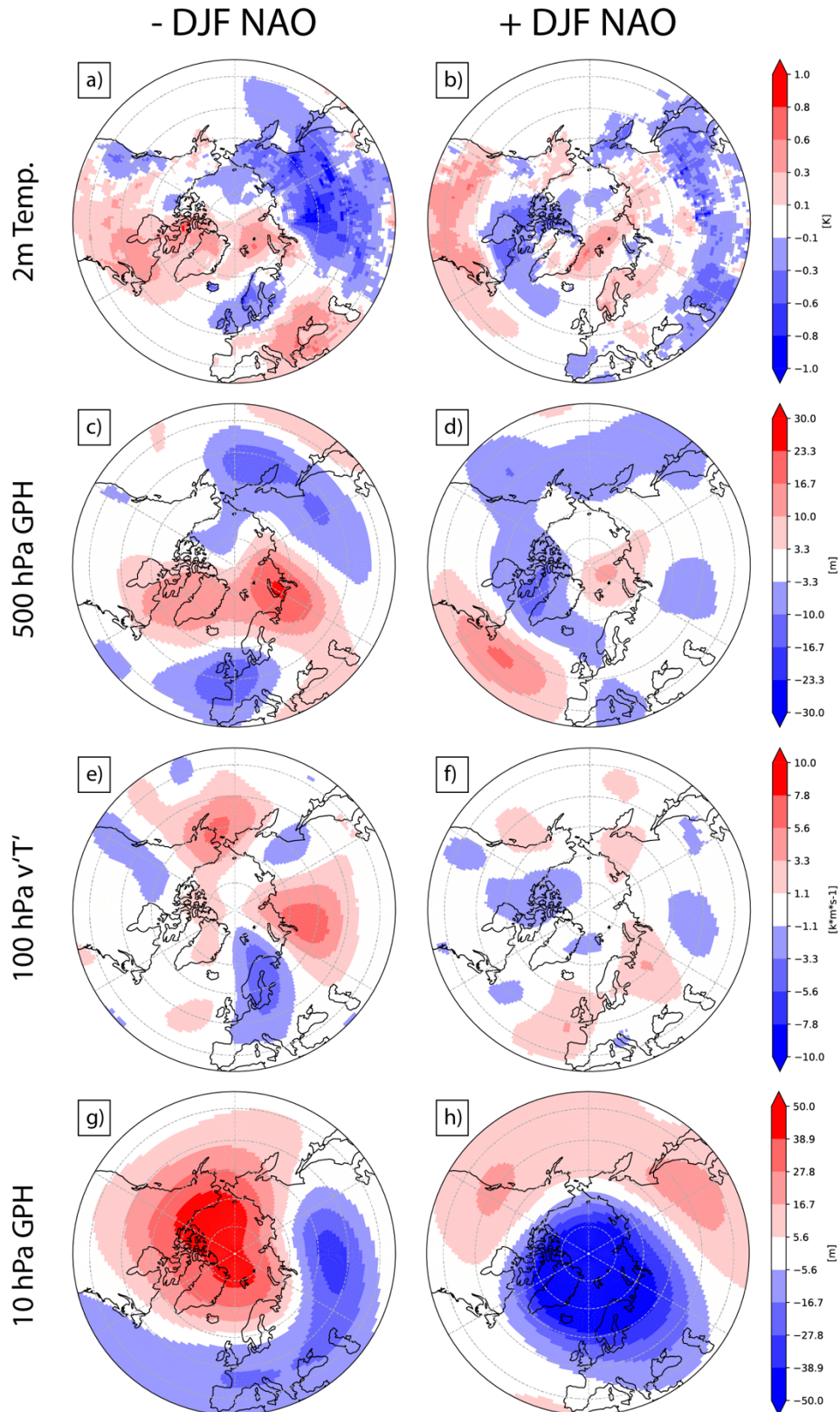
807 *Figure 7: Zonal-mean cross-section of left) zonal wind anomalies and right) temperature anomalies for*  
 808 *the period 1901-2010 between high-dipole and low-dipole ASF-20C EXP ensemble means. Shading*  
 809 *indicates 90% significance level.*





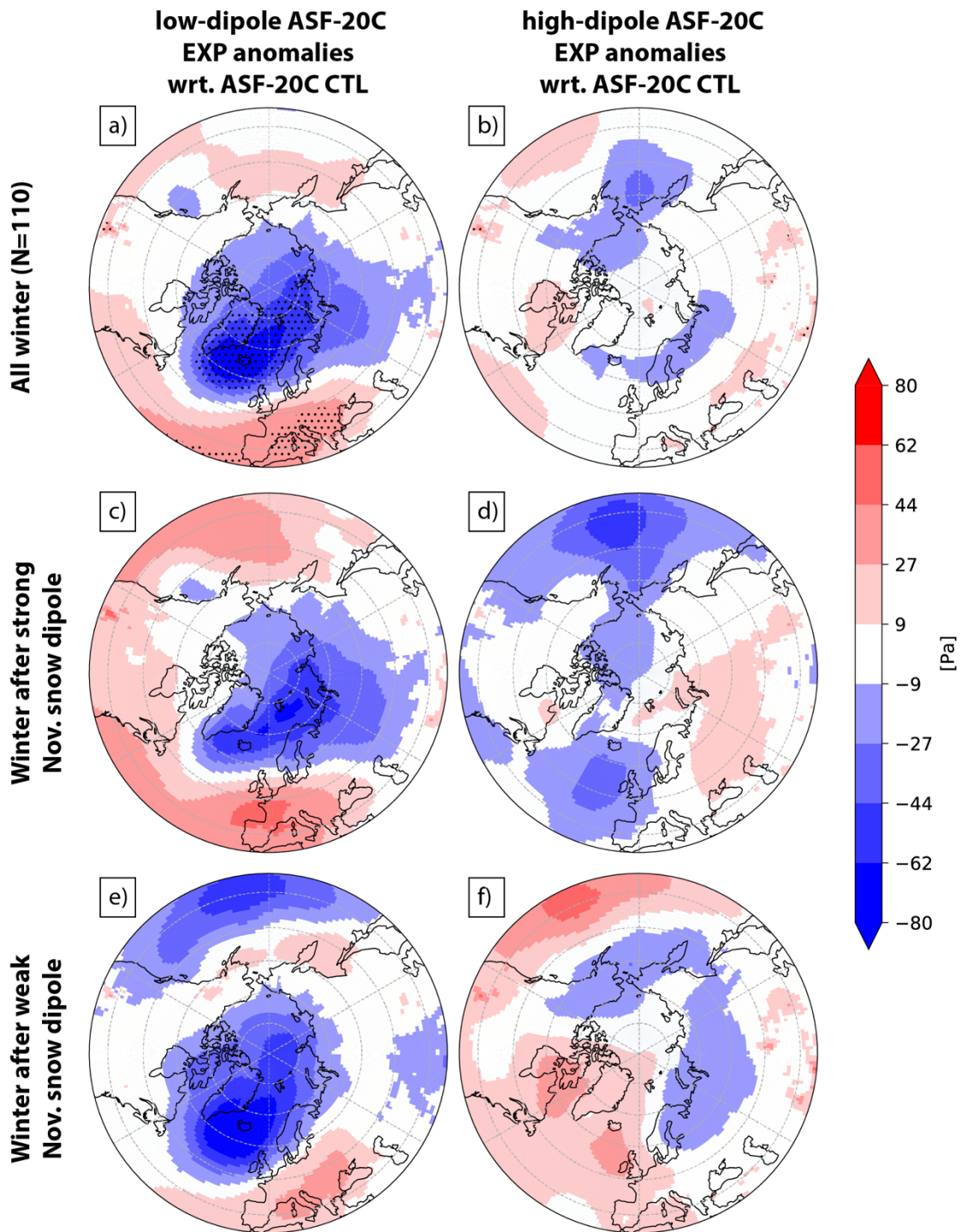
810

811 *Figure 8: Hovmöller diagram of daily mean predicted 500 hPa geopotential height anomalies for the*  
 812 *period 1901-2010 averaged for the latitude band 60°-70°N difference between high-dipole and low-*  
 813 *dipole ASF-20C EXP ensemble means. Stippled areas represent 90% significance. Days from NOV 1<sup>st</sup>*  
 814 *are indicated on y-axis.*



815

816 *Figure 9: Climate anomaly composites of predicted December fields after which a positive snow dipole*  
 817 *forcing preceded a negative DJF NAO signal (a,c,e,g) or a positive DJF NAO signal (b,d,f,i)(selection*  
 818 *of years based on Figure 1d): a&b) 2m temperature, c&d) 500 hPa geopotential heights, e&f) 100hPa*  
 819 *meridional eddy temperature flux, g&h) 10 hPa geopotential heights. Anomalies are based on ASF-*  
 820 *20C EXP high-low snow dipole ensemble mean data.*



821

822 *Figure 10: Mean sea level pressure [Pa] DJF anomalies for the period 1901-2010 between a) low-*  
 823 *dipole ASF-20C EXP ensemble mean and ASF-20C CTL ensemble mean (subsamped from 21 CTL*  
 824 *members) and b) high-dipole ASF-20C EXP ensemble mean and ASF-20C CTL ensemble mean*  
 825 *(subsamped from 21 CTL members). Stippled areas represent 90% significance. c) Represents*  
 826 *differences between low-dipole ASF-20C EXP ensemble mean and ASF-20C CTL ensemble mean DJF*  
 827 *seasons after positive snow dipole in ERA20C 1<sup>st</sup> November snow depth (see Figure 1a). d) as c) but*  
 828 *for the high-dipole ASF-20C EXP ensemble mean. e) and f) same as c) and d) but for seasons after*  
 829 *negative snow dipole in ERA20C 1<sup>st</sup> November snow depth.*

830